

**POLITECNICO**  
**MILANO 1863**

Design of an additive manufactured  
propulsive system based on H<sub>2</sub>O<sub>2</sub> and RP-1

Team: **PropulsionWhateverItTakes**

ID	Surname	Name
10675538	Arioli	Andrea
10566736	Bellicosso	Davide
10671536	Pecchini	Luca
10620335	Picozzi	Riccardo
10603740	Prosperi	Alessio
10614648	Rambaldi	Riccardo
10618360	Tognola	Paolo
10659503	Tomassi	Emanuele
10612897	Zamblera	Davide

Course of Space Propulsion  
M.Sc Space Engineering  
Academic Year 2021-2022

# Abstract

This report aims at presenting the designing a liquid propulsion unit based on H<sub>2</sub>O<sub>2</sub> and RP-1, which shall provide a thrust of 100N in vacuum. The system is characterised by a liquid injection system and a blow-down architecture. The motor must provide at least 50% of the initial nominal 100N thrust for 100 seconds of burning. The initial combustion chamber pressure is set at 20 bar and the nozzle expansion ratio at 80. The first step of the sizing involves the nozzle and the combustion chamber (including the injection plate), followed by the analysis of the specific impulse and thrust variation as a function of time. Lastly, an evaluation of manufacture-related aspects is performed, and a Montecarlo simulation is carried out to estimate the uncertainty boundaries affecting the thrust due to the industrial processes employed to realise the motor by additive manufacturing of the combustion chamber and nozzle.



Figure 1: 3D view of designed propulsion system

# Contents

<b>1 Nozzle geometry and related losses</b>	<b>1</b>
1.1 Conic nozzle . . . . .	1
1.1.1 Mach number assumption . . . . .	1
1.1.2 Contraction ratio assumption . . . . .	2
1.2 Rao nozzle . . . . .	2
1.2.1 Minimum length approach . . . . .	2
1.2.2 Max performance approach . . . . .	2
<b>2 Combustion chamber design</b>	<b>3</b>
2.1 Combustion chamber preliminary design . . . . .	3
2.1.1 $L^*$ assumption . . . . .	3
2.1.2 First and second iteration . . . . .	3
2.1.3 Shapiro model . . . . .	4
2.2 CEA analysis . . . . .	4
2.2.1 First iteration: CC infinite area . . . . .	4
2.2.2 Data gathering and optimization search . . . . .	5
2.2.3 Second iteration: CC finite area . . . . .	6
2.3 Design of injectors . . . . .	6
2.4 Regenerative cooling, heat transfer and thermal analysis . . . . .	6
2.4.1 Steady state thermal analysis . . . . .	6
2.4.2 Assumptions with regenerative cooling . . . . .	6
<b>3 Blowdown Model</b>	<b>7</b>
3.1 Isoentropic and isothermal expansion analysis . . . . .	7
3.1.1 Performance ceiling and floor . . . . .	7
3.1.2 Design choice . . . . .	7
3.2 Pressure losses estimation . . . . .	7
3.3 Ballistic simulation with pressure losses . . . . .	8
3.4 Optimization of the initial conditions . . . . .	8
3.4.1 Variables, Constraint, Objective function . . . . .	8
3.4.2 Optimization results . . . . .	9
3.4.3 Detail of the numerical model and scripts . . . . .	9
<b>4 Statistical analysis</b>	<b>10</b>
4.1 Montecarlo simulation . . . . .	10
4.2 Determination of uncertainties . . . . .	10
4.3 Sensitivity analysis . . . . .	11
4.4 Extension to 10N and 1000N thrusters . . . . .	11
<b>5 Additive manufacturing</b>	<b>12</b>
<b>Bibliography</b>	<b>VIII</b>
<b>A CAD modelling</b>	<b>X</b>
<b>B Literature review of injection and combustion with liquid H<sub>2</sub>O<sub>2</sub></b>	<b>XII</b>

<b>C Preliminary analysis</b>	<b>XIII</b>
C.1 Tables and graphs . . . . .	XIII
C.2 Nozzle and chamber geometry calculation . . . . .	XIV
C.2.1 Main equations . . . . .	XIV
C.2.2 Matlab script . . . . .	XIV
C.3 CEA analysis . . . . .	XVII
C.3.1 Optimal NASA-CEA analysis . . . . .	XVIII
<b>D Thermal analysis</b>	<b>XIX</b>
<b>E Blowdown model</b>	<b>XX</b>
E.1 Pressure losses estimation . . . . .	XX
E.1.1 Equations . . . . .	XX
E.1.2 Figures and Matlab function . . . . .	XX
E.2 Blowdown analysis . . . . .	XXII
E.2.1 Mathematical equations and discretized model . . . . .	XXII
E.2.2 Matlab script . . . . .	XXII
E.2.3 Tanks sizing . . . . .	XXV
E.3 Optimization of initial variables . . . . .	XXV
E.3.1 Variables . . . . .	XXV
E.3.2 Variables' ranges . . . . .	XXV
E.3.3 Constraints . . . . .	XXVI
E.3.4 Objective function . . . . .	XXVI
E.3.5 Optimizer . . . . .	XXVI
<b>F Statistical analysis</b>	<b>XXVII</b>
F.1 Montecarlo initialization and post-processing . . . . .	XXVII
F.2 Simulation with uncertainties . . . . .	XXVIII
F.3 Results of the sensitivity analysis . . . . .	XXX

# List of Figures

1	3D view of designed propulsion system . . . . .	I
2.1	Combustion chamber length over contraction ratio . . . . .	3
2.2	Shapiro simulation with initial CC design . . . . .	4
2.3	Shapiro simulation with final CC design . . . . .	4
2.4	CEA simulation results . . . . .	5
3.1	Isothermal vs Adiabatic expansion . . . . .	7
3.2	Iterations of the optimization function . . . . .	9
3.3	Results of the optimization . . . . .	9
4.1	Results of Montercarlo simulation (black lines: max and min boundary values) . . . . .	10
5.1	Shape-forming capability of different AM processes (DMLS=Direct Metal Laser Sintering, LPD=Laser Powder Deposition, EBWD=Electron Beam Wire Deposition, GMAW=Gas Metal Arc Welding) [10] . . . . .	12
A.1	Total CAD model of the designed propulsion system . . . . .	X
A.2	Cut-off view of AM injector plate design . . . . .	X
A.3	Cut-off view of separate injector plate design . . . . .	XI
A.4	Injector design . . . . .	XI
C.1	Area and velocity ratios as function of pressure ratio for the diverging section of a supersonic nozzle. . . . .	XIII
C.2	Parabola angles as function of expansion ratio. . . . .	XIII
C.3	Theoretical Performance of Liquid Rocket Propellant Combinations . . . . .	XIV
C.4	Combustion chamber temperature . . . . .	XVII
C.5	Exit temperature and Thrust coefficient . . . . .	XVII
C.6	CEA analysis . . . . .	XVII
D.1	Wall temperatures with radiative cooling . . . . .	XIX
D.2	Heat transfer with radiative cooling . . . . .	XIX
E.1	Moody diagram . . . . .	XX
F.1	Throat diameter as variable parameter REFINED . . . . .	XXX
F.2	Throat diameter as variable parameter NOT REFINED . . . . .	XXX
F.3	Feeding lines diameter as variable parameter . . . . .	XXXI
F.4	Injectors diameters as variable parameter . . . . .	XXXI

# List of Tables

2.1	Preliminary combustion chamber results, two iterations. $L^* = 2.1336m$ . . . . .	4
2.2	Data for CEA simulation . . . . .	5
2.3	Composition at exit section . . . . .	5
2.4	Main parameters . . . . .	6
4.1	Nominal values . . . . .	10
4.2	Standard deviation at $1\sigma$ . . . . .	10
4.3	Relative standard variation of the design parameters . . . . .	11
4.4	Std of final thrust with different uncertainties (App. F.3) . . . . .	11
E.1	Tanks sizing results . . . . .	XXV

# List of Symbols

Variable	Description	Unit
$\alpha$	Initial convergent angle	◦
$\beta$	Final convergent angle	◦
$\gamma$	Heat specific ratio	—
$\gamma_{poly}$	Polytropic transformation coefficient	—
$\Delta P$	Pressure loss	Pa
$\Delta t$	Time interval	s
$\epsilon$	Expansion ratio	—
$\epsilon_c$	Contraction ratio	—
$\theta_i$	Initial RAO convergent angle	◦
$\theta_e$	Final RAO convergent angle	◦
$\lambda$	Divergent section efficiency	—
$\lambda_{dist}$	Distributed friction coefficient	—
$\mu$	Dynamic viscosity	mP
$\rho$	Density	kg/m <sup>3</sup>
$\rho_p$	Propellant density	kg/m <sup>3</sup>
$A$	Section area	m <sup>2</sup>
$A_c$	Combustion chamber area	m <sup>2</sup>
$A_t$	Throat area	m <sup>2</sup>
$c^*$	Characteristic velocity	m/s
$CC$	Combustion chamber	—
$C_d$	Discharge coefficient	—
$C_f$	Fanning friction coefficient	—
$c_p$	Specific heat capacity	J/kgK
$c_t$	Thrust coefficient	—
$D$	Diameter	m
$D_c$	Combustion chamber diameter	m
$D_e$	Nozzle exit diameter	m
$D_{FU}^{feed}$	Fuel feeding line tubes diameter	m
$D_{OX}^{feed}$	Oxidizer feeding line tubes diameter	m
$D_{FU}^{inj}$	Fuel injector hole diameter	m
$D_{OX}^{inj}$	Oxidizer injector hole diameter	m
$D_t$	Nozzle throat diameter	m
$D_t$	Throat section diameter	m
$I_{sp}$	Specific impulse	s
$I_{vac}$	Vacuum specific impulse	s

Variable	Description	Unit
$K_{conc}$	Concentrated pressure loss coefficient	—
$K_{dist}$	Distributed pressure loss coefficient	—
$K_{fuel}$	Fuel pressure loss coefficient	—
$K_{ox}$	Oxidizer pressure loss coefficient	—
$L_c$	Combustion chamber length	$m$
$L_{conic-conv}$	Nozzle convergent length	$m$
$L_{conic-div}$	Nozzle divergent length	$m$
$L_{RAO-ref}$	RAO nozzle divergent reference length	$m$
$L^*$	Combustion chamber characteristic length	$m$
$M$	Mach number	—
$M_c$	Combustion chamber mach number	—
$M_{prop}$	Propellant mass	$Kg$
$\dot{m}$	Mass flow rate	$Kg/s$
$\dot{m}_{fuel}$	Fuel mass flow rate	$Kg/s$
$M_m$	Molar mass	$g/mol$
$\dot{m}_{ox}$	Oxidizer mass flow rate	$Kg/s$
$O/F$	Oxidizer to fuel ratio	—
$P_c$	Combustion chamber pressure	$bar$
$P_e$	External pressure	$Pa$
$P_{fuel}$	Fuel pressure	$Pa$
$P_{gas}$	Gas phase pressure	$Pa$
$P_{ox}$	Oxidizer pressure	$Pa$
$P_0$	Total pressure	$Pa$
$R_u$	Universal gas constant	$J/molK$
$T$	Thrust	$N$
$T_0$	Total temperature	$^\circ$
$T_{amb}$	Ambient temperature	$K$
$T_{gas}$	Gas temperature	$K$
$T_{vac}$	Thrust at vacuum condition	$N$
$T_{conic-1D}$	One-dimensional thrust for conic nozzle	$N$
$T_{conic-2D}$	Two-dimensional thrust for conic nozzle	$N$
$t_s$	Residence time	$s$
$V_c$	Combustion chamber volume	$m^3$
$V_{gas}$	Volume of gas	$m^3$
$V_{prop}$	Volume of propellant	$m^3$
$V_{g_{fuel}}$	Volume of helium in the fuel tank	$m^3$
$V_{g_{ox}}$	Volume of helium in the oxidizer	$m^3$
$\dot{m}_p$	Propellant mass flow rate	$Kg/s$
$\dot{m}_{fuel}$	Fuel mass flow rate	$Kg/s$
$\dot{m}_{ox}$	Oxidizer mass flow rate	$Kg/s$

# Chapter 1

## Nozzle geometry and related losses

### 1.1 Conic nozzle

Starting from a reference value of  $\gamma = 1.19$  from literature (Fig C.3) and an expansion ratio  $\epsilon$  fixed from requirements, the ratio  $(\frac{P_e}{P_c})$  was evaluated through a graphical method (Fig C.1). Then, to refine the result,  $(\frac{P_e}{P_c})$  was iteratively inserted inside equation Eq. 1.1 to obtain  $\epsilon = 80$ .

$$\frac{1}{\epsilon} = \frac{A_t}{A_e} = \left( \frac{\gamma + 1}{2} \right)^{\frac{1}{\gamma-1}} \left( \frac{P_e}{P_c} \right)^{\frac{1}{\gamma}} \sqrt{\frac{\gamma + 1}{\gamma - 1} \left[ 1 - \left( \frac{P_e}{P_c} \right)^{\frac{\gamma-1}{\gamma}} \right]} \quad (1.1)$$

Thereafter, the final value of  $(\frac{P_e}{P_c})$  was calculated with the value of  $\gamma = 1.2083$ , which was reverse-engineered from the NASA-CEA results in the combustion chamber.

Thrust coefficient  $c_F$  was evaluated through the Eq. 1.2:

$$c_F = \sqrt{\frac{2\gamma^2}{\gamma-1} \left( \frac{2}{\gamma-1} \right)^{\frac{\gamma+1}{\gamma-1}} \left[ 1 - \left( \frac{P_e}{P_c} \right)^{\frac{\gamma-1}{\gamma}} \right]} + \frac{P_e}{P_c} \cdot \epsilon \quad (1.2)$$

The throat area  $A_t$  was then evaluated starting from an initial value of thrust equal to the nominal one of  $100 \text{ N}$ , with the equation  $A_t = \frac{T}{P_c \cdot c_F}$ . This value was refined after computing the 2D losses of the selected design of the nozzle resulting in a final throat area of  $2.61367 \cdot 10^{-5} \text{ m}^2$ . The external area is  $A_e = A_t \cdot \epsilon = 0.0021 \text{ m}^2$ , obtained from the expansion ratio definition.

It was decided to opt for a conic nozzle as the first iteration of the design process, with  $\alpha = 15$  and  $\beta = 45$ , taken as reference values from literature. The efficiency of the divergent part of the nozzle was computed with Eq. 1.3:

$$\lambda_{conic} = \frac{1 + \cos(\alpha)}{2} = 0.9830 \quad (1.3)$$

Knowing the losses, the 1D thrust was computed in Eq. 1.4 assuming that the bi-dimensional thrust is the nominal one of  $100 \text{ N}$ :

$$T_{conic-1D} = \frac{T_{conic-2D}}{\lambda_{conic}} = 101.7332 \text{ N} \quad (1.4)$$

Subsequently, the length of the divergent of the nozzle was evaluated (Eq. 1.5):

$$L_{conic-div} = \frac{D_e - D_t}{2 \cdot \tan(\alpha)} = 0.0855 \text{ m} \quad (1.5)$$

#### 1.1.1 Mach number assumption

The first iteration to compute the geometry of the convergent part of the nozzle was completed assuming a Mach number in the combustion chamber of  $0.3$  from literature [1]. Subsequently the area of the combustion chamber  $A_c$  was evaluated in Eq. 1.6:

$$A_c = \left( \frac{A_t}{M_c} \right) \cdot \sqrt{\left[ \frac{2}{\gamma + 1} \left( 1 + \frac{\gamma - 1}{2} \cdot M_c^2 \right) \right]^{\frac{\gamma + 1}{\gamma - 1}}} \quad (1.6)$$

The diameter  $D_c$  of the combustion chamber was 0.0083 m and the contraction ratio  $\epsilon_c = \frac{A_c}{A_t}$  was 2.0715. The length of the convergent part of the nozzle was computed in Eq. 1.7:

$$L_{conic-conv} = \frac{D_c - D_t}{2 \cdot \tan(\beta)} = 0.0013m \quad (1.7)$$

The total length of the conic nozzle with the  $M = 0.3$  assumption was 0.0868 m

### 1.1.2 Contraction ratio assumption

Having a combustion chamber with a diameter of 8.3 mm would be not optimal since, using the values of  $L^*$  found in the literature [1], the CC length would be of 1.0299 m, introducing not-negligible losses of total pressure due to friction (see Fig. 2.2).

As explained in the 2.1.2 section, it was decided to opt for a higher contraction ratio  $\epsilon_c = 18$ , and to use it for the whole design of the system.

It was possible to compute the area of the CC and so its diameter  $D_c = 0.0245$  m. Furthermore, from the implicit equation Eq. 1.6 it was calculated  $M_c = 0.0329$  with *fsolve*. The length of the convergent part of the nozzle computed was  $L_{conic-conv} = 0.0094$  m and the total length of the conic nozzle with the  $\epsilon_c = 18$  assumption was 0.0949 m

## 1.2 Rao nozzle

### 1.2.1 Minimum length approach

The computation of the RAO nozzle started from the conical one with  $\alpha = 15^\circ$ . The first approach selected was the *Minimum length* one with the length of the divergent equal to 60% of the divergent of the conic nozzle, taken as reference  $L_{RAO-ref} = L_{conic-div} = 0.0855$  m. The length of the divergent was  $L_{RAO-div} = 0.6 \cdot L_{RAO-ref} = 0.0513$  m.

With a graphical method from the RAO curves (App. C.1),  $\theta_i = 38.5^\circ$  and  $\theta_e = 12.5^\circ$  were selected. It was possible to compute the new  $\alpha = 24.07^\circ$  with the inverse of the equation 1.5 and subsequently the efficiency of the divergent  $\lambda$  with the Eq. 1.8:

$$\lambda_{RAO-ML} = \frac{1 + \cos(\frac{\alpha+\theta_e}{2})}{2} = 0.9748 \quad (1.8)$$

The total length of the RAO nozzle with the *Minimum length approach*, considering the length of the convergent equal to the one evaluated in the conic nozzle, was 0.0607 m.

### 1.2.2 Max performance approach

It was decided to improve the nozzle from the efficiency point of view, so the *Max performance approach* was selected as the definitive design choice for the system. With this approach, the length of the divergent was taken equal to the one of the conic nozzle, so  $L_{RAO-div} = L_{conic-div} = 0.0855$  m.

With a graphical method from the RAO curves (App. C.1),  $\theta_i = 31^\circ$  and  $\theta_e = 4.25^\circ$  were selected. The divergent angle  $\alpha = 15$  was equal to the one selected for the conic nozzle, and the efficiency of the divergent  $\lambda$ , evaluated with the Eq. 1.8, was 0.9930. As expected, choosing a RAO nozzle with the length of the divergent equal to the reference one from the conic nozzle design improves the efficiency of the system reducing the 2D losses.

# Chapter 2

## Combustion chamber design

### 2.1 Combustion chamber preliminary design

Starting from an assumed value of contraction ratio, the combustion chamber section area was evaluated as  $A_c = \epsilon_c A_t$ , where the throat area  $A_t = 26.1367 \text{ mm}^2$  used was the one computed in Chapter 1. The volume of the combustion chamber was then evaluated through the definition of the characteristic length  $L^* = \frac{V_c}{A_t}$ .

#### 2.1.1 $L^*$ assumption

The characteristic length,  $L^*$ , is an experimental parameter which defines the proper volume of the combustion chamber to assure the completion of the combustion of the propellants. In fact, it is directly proportional to the residence time of the propellant couple in the combustion chamber through  $L^* = \frac{\dot{m}_p}{\rho_p A_t} t_s$ . The acceptable values of characteristic length for the couple H<sub>2</sub>O<sub>2</sub>/RP-1 were found in literature with the addition of a catalyst bed [1], ranging from 1.52 m to 1.78 m.

In order to meet the requirement of a liquid injection, the catalyst bed was not considered for the evaluated system since it decomposes the HTP in gaseous products to boost the combustion and permit auto-ignition. The combustion is less effective and slower without the catalyst and needs a higher residence time. Therefore, an assumed safety factor of 1.2 was used for the highest value of  $L^*$  which increases the  $t_s$  of a 20%, leading to a characteristic length of 2.1336 m and a residence time of 3.3 ms. The assumption made for including the liquid injection system should be evaluated through a conveniently prepared firing test.

#### 2.1.2 First and second iteration

For the first sizing of the combustion chamber, an  $\epsilon_c = 2.0715$  was used, obtained from an assumed  $M_c = 0.3$  inside the combustion chamber. The resulting dimensions described a shape of the combustion chamber with the longitude size much bigger than the diameter of the section area. In order to reduce both the length of the CC and the total pressure losses due to friction, as explained in the 2.1.3 section, higher  $\epsilon_c$  were evaluated. From literature, it was discovered that for small propulsion systems, a higher contraction ratio could be used, even until a value of 50 [2].

Considering the evolution of the combustion chamber length over the contraction ratio, a value of 18 was chosen, since it lies just before the visible trend toward an asymptotic value (Fig.2.1).

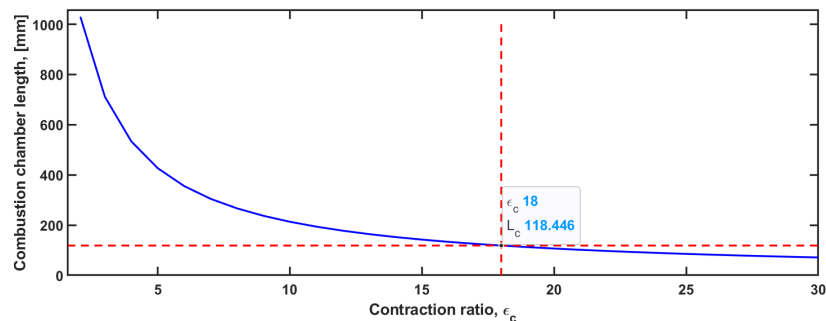


Figure 2.1: Combustion chamber length over contraction ratio

$\epsilon_c$	$D_c[\text{mm}]$	$V_c[\text{mm}^3]$	$L_c[\text{mm}]$	$Ma$
2.0715	8.3449	5.6333e+4	1029.985	0.3
18	24.5990	5.6333e+4	118.4463	0.0329

Table 2.1: Preliminary combustion chamber results, two iterations.  $L^* = 2.1336m$

### 2.1.3 Shapiro model

The Shapiro equations for the combustion chamber, with constant area, were implemented and solved numerically with MATLAB with the 5<sup>th</sup> order Runge-Kutta method.

$$\frac{dM^2}{dx} = \gamma M^4 \frac{1 + \frac{\gamma-1}{2} M^2}{T_0(1 - M^2)} \frac{4C_f}{D} + M^2 \frac{(1 + \gamma M^2)(1 + \frac{\gamma-1}{2} M^2)}{1 - M^2} \frac{dT_0}{dx} \quad (2.1)$$

$$\frac{dP_0}{dx} = -p_0 \gamma \frac{M^2}{2} \left( \frac{4C_f}{D} + \frac{dT_0}{T_0} \right) \quad (2.2)$$

Using the first design of the combustion chamber, the total pressure losses were very high since the CC was very long, slim and had a non negligible initial Mach number (Fig. 2.2).

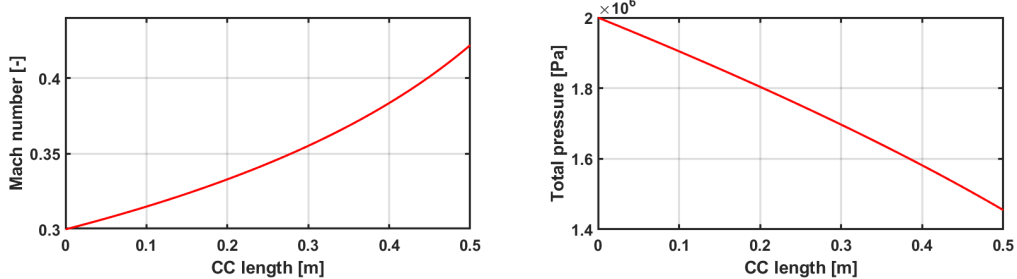


Figure 2.2: Shapiro simulation with initial CC design

By instead using the final design of the combustion chamber, it was possible to assume the chamber to be isoentropic, since the total pressure loss over the CC is in the order of 0.01 % (Fig. 2.3).

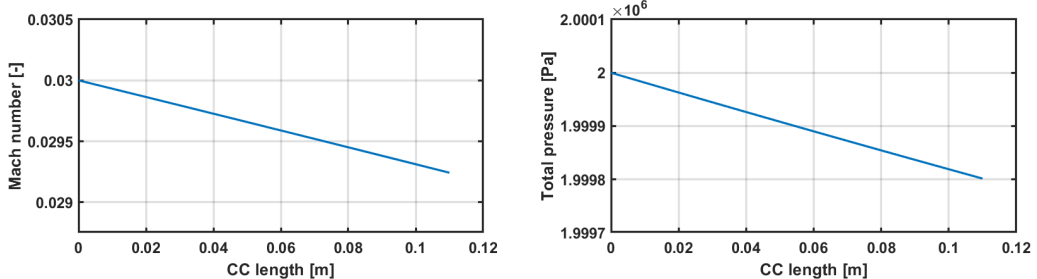


Figure 2.3: Shapiro simulation with final CC design

After analysing these results, it was decided that the Shapiro equation could be accurately approximated with an isoentropic model.

## 2.2 CEA analysis

### 2.2.1 First iteration: CC infinite area

A CEA analysis on the initial motor firing condition was implemented: the objective of this simulation was to obtain an insight on possible  $I_{vac}$ , typical combustion temperatures and O/F operating points for the selected propellants. The O/F ratio is defined as mass flow rate of oxidizer (the diluted H<sub>2</sub>O<sub>2</sub>) over mass flow rate of fuel (RP-1). The performance parameter selected to be maximized was the specific impulse, moreover other data as  $c^*$  and  $c_t$  were gathered for future use in the rest of the design.

## 2.2.2 Data gathering and optimization search

The CEA simulation was performed with the three main models for reactive flow in the nozzle, in particular the Bray model was considered with the freezing point at the throat. Then, the results were critically interpreted to find the most accurate model. Initially a simulation with an infinite combustion chamber area has been utilized. The entry temperature of oxidizer and fuel at ambient temperature was preliminary assumed before considering any regenerative cooling system. After a proper design of the cooling mechanism, the corrected temperature of oxidizer after the heat exchange should be considered. The input to the simulation is summarized in Tab. 2.2:

$$p_0 = 20\text{bar} \quad \epsilon = 80$$

Reactant	WT Fraction	Energy KJ/Kg-mol	Temperature K
H <sub>2</sub> O <sub>2</sub> (L)	0.875 (ox)	-187780.000	298.15
H <sub>2</sub> O(L)	0.125 (ox)	-285830.088	298.15
RP-1	1 (fuel)	-24717.700	298.15

Table 2.2: Data for CEA simulation

The results of the simulation are visualised in Fig. 2.4

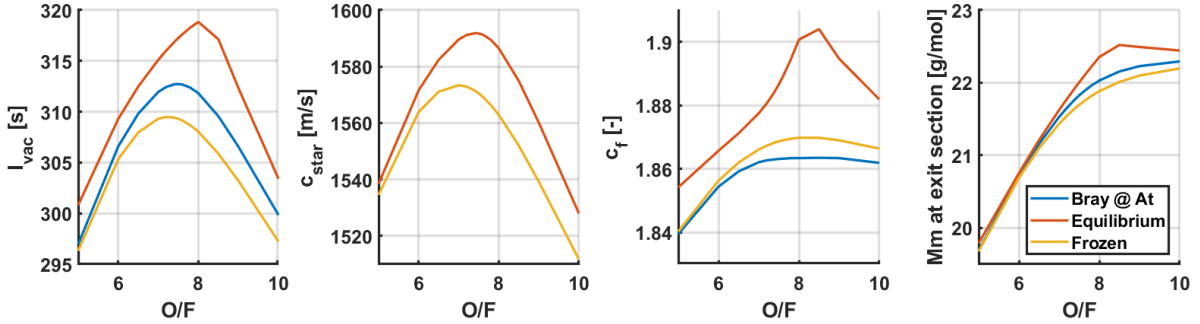


Figure 2.4: CEA simulation results

Given that the O/F obtained from the simulations (Fig. 3.3) is almost constant ( $\approx 10^{-3}$  variation), the  $I_{sp}$  and  $c^*$  are constant. Given the fixed geometry, with  $\epsilon = 80$ , the pressure ratio is constant and so the thrust coefficient  $c_T$ . It can be assumed constant  $I_{sp}$  during the firing.

It can be noted that the different models for the flow in the nozzle yield similar results, with equilibrium having the best results as it permits recombination reactions while the propellants cool down. The main differences are with equilibrium expansion with O/F  $\approx 3$ , as it could be seen from Fig. C.6, because at lower O/F the expanded flow has a lower temperature than those with higher O/F. This triggers recombination reactions in the flow and results in a higher molecular mass and a higher temperature with respect to other flow models due to these reactions being exothermic. Nevertheless, the Bray model [3] is the most accurate and the one that was considered for the whole analysis since the combustion involves the production of water, and the freezing point is located at the throat. (Table. 2.3, note water as a main product).

CO	CO <sub>2</sub>	H	H <sub>2</sub>	H <sub>2</sub> O	O	OH	O <sub>2</sub>
0.03335	0.15036	0.00133	0.02755	0.77554	0.00025	0.00873	0.00288

Table 2.3: Composition at exit section

One of the main results of the simulation is inherent to the combustion chamber temperature, which in the operative range maintains values around 2600K (Fig. C.6). It is then paramount to investigate this temperature level's thermal constraints and main challenges to the chamber's thermo-mechanical properties.

From these simulations it was noted that the operating point of our engine, to maximize the specific impulse at vacuum, was in a range between 7.45 and 7.5. The resulting main parameters, operating at this ratio, are listed in Tab. 2.4.

$I_{vac}$ [s]	$c^*$ [m/s]	$c_t$	$M_m$ [g/mol]	$T$ [K]
312.716	1591.7	1.8631	21.695	2675.99

Table 2.4: Main parameters

Then other gas properties could be derived from this data. Considering the exit composition of a frozen flow, which will be equal to the composition at chamber exit, the  $c_p$  of the mixture could be found by gathering data from the Penner tables. Transport properties were also computed.

$$c_p = 52.635 \text{ kJ/mol K} \quad \gamma = \frac{1}{1 - \frac{R_u}{c_p}} = 1.2083 \quad \mu = 0.96373 mP \quad (2.3)$$

### 2.2.3 Second iteration: CC finite area

As the combustion chamber is not infinite but it has a finite contraction ratio, a simulation with  $A_c/A_t = 18$  was computed. As CEA can do this kind of modelling only with an equilibrium flow the results were then compared with an infinite chamber and equilibrium model. The difference on all the major performance parameters was negligible and so the results of the CEA with infinite chamber were used for the rest of the model.

## 2.3 Design of injectors

Firstly, the pressure loss due to the injection was assumed as high as 1/5 of the combustion chamber pressure. Then, the area needed for the injection of fuel and oxidizer was found inverting the formula:

$$C_d = \frac{\dot{m}}{A\sqrt{2\rho\Delta P}} \quad (2.4)$$

Starting from standard design [4], the model chosen is a short tube with rounded entrance because it was the only one granting 2 injectors for type, with a diameter of 0.5 mm and a Cd of 0.7. The number of injectors was chosen as the minimum between the fuel and the oxidizer, resulting in 1.11 and 6.52, rounded to 2 and 7. It was necessary to redesign both injectors: in order to pass from 7 injectors to 2 for the oxidizer and to fill the discrepancy between the area needed for 1.1 injectors and 2. The redesign led to 0.9026 mm and 0.3726 mm diameters respectively. In conclusion, chosen the double impinging configuration and the inclination of the fuel injector equal to  $30^\circ$ , it was obtained, through the inelastic collision formula, an inclination of the oxidizer injector of around  $4.9^\circ$ .

## 2.4 Regenerative cooling, heat transfer and thermal analysis

### 2.4.1 Steady state thermal analysis

An initial steady-state thermal analysis was performed by assuming a radiative passive cooling system with the Rocket Propulsion Analysis software [5] (see App. D).

The walls temperature were far higher than the maximum allowed by the material [6] so this solution could not be implemented.

### 2.4.2 Assumptions with regenerative cooling

Given a lack of information about the surroundings of the combustion chamber, an accurate heat transfer and thermal analysis could not be performed to pinpoint the exact heat flux trough the walls accurately. A working regenerative cooling system composed by a radiator, a regulation valve and an electric pump with an additional fluid to dissipate heat has been hypothesized. It has been estimated the  $\frac{\partial T_0}{\partial dx}$  with a 5% total temperature loss over the length of the combustion chamber [4].

# Chapter 3

## Blowdown Model

### 3.1 Isoentropic and isothermal expansion analysis

#### 3.1.1 Performance ceiling and floor

The isothermal and adiabatic gas expansions are the theoretical ceiling and floor, respectively, of the work efficiency of a real polytropic expansion.

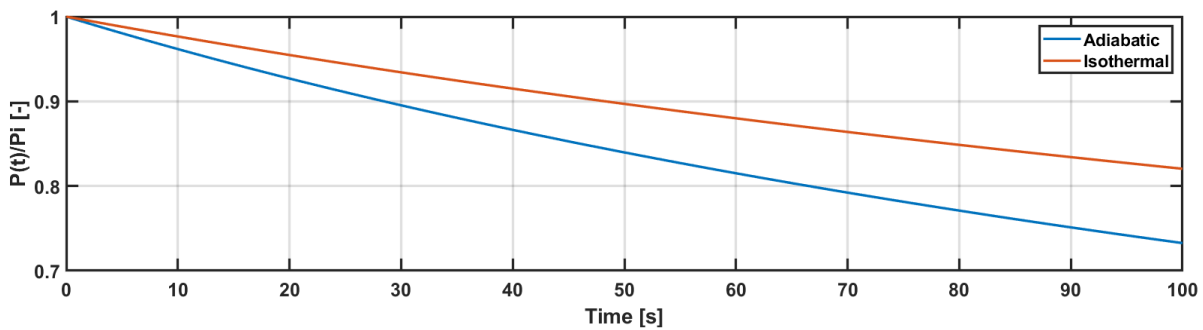


Figure 3.1: Isothermal vs Adiabatic expansion

This means that the real expansion is a trade-off between these two boundary conditions (Fig. 3.1).

#### 3.1.2 Design choice

An adiabatic condition would be a good approximation for a fast transformation and would be a conservative choice, because of the underestimation of the real performance of the system. The adiabatic transformation leads to a cooling of the pressurizing gas, which could cause the freezing of the oxidizer [7], limiting the maximum blowdown ratio reachable.

Since regenerative cooling has been supposed, the hot cooling fluid at the combustion chamber outlet could be used to keep the gas temperature inside of the fuel and oxidant tanks constant, allowing an isothermal transformation and avoiding the freezing problem. This thermal configuration increases the overall performance of the system, allowing a blowdown ratio increase and a subsequent minimization of the tank volume and total system mass.

### 3.2 Pressure losses estimation

In order to describe the performance variation during burn time properly, a pressure loss investigation of the feeding lines must be performed. The goal is to find an equivalent pressure loss coefficient for each feeding line, in order to obtain an explicit relation between pressure drop and mass flow rate as follows:

$$\Delta P = K \cdot \dot{m}^2 \quad (3.1)$$

To estimate these parameters different pressure losses have been considered:

1. Distribute losses in the piping system
2. Concentrated losses in check valves and latch valves

3. Injector losses
4. Dynamic pressure losses

Firstly the valves were chosen, prioritising the smallest and lightest models commercially available and compliant with our application. The valves concentrated losses have been derived from the relative data-sheets [8]. Once the valves have been selected, the piping system has been roughly sized, selecting a diameter in accordance with valves interfaces, while the length has been estimated from a preliminary CAD model (App. A) of the complete system.

The distributed losses of the piping system have been computed considering the Reynolds number of each fluid and the relative roughness of the pipes selecting a drawn tubing technology. Inserting these values in the Moody Diagram (Fig. E.1), the friction coefficient has been graphically estimated.

The injectors losses have been derived from the precedent injectors sizing, and the equations have been manipulated to find specific relations. 3.1. The dynamic pressure losses have been estimated with the assumption of constant density of the fluid, finding the correlation with mass flow rate.

### **3.3 Ballistic simulation with pressure losses**

Starting from nominal conditions, an iterative analysis of the performance evolution during time has been performed. For every time step, the amount of fuel and of oxidizer used and the expansion of the gaseous He in each tank were computed. Using the perfect gas assumption and the previously-defined polytropic transformation, the pressure of the tanks were obtained. With these new estimated tanks pressure and knowing the pressure losses in the system, a non-linear system of equation was solved to obtain fuel and oxidizer mass flow rates and combustion chamber pressure (Eq. E.9). The iterative method runs until the total burn time is reached or the propellant is finished.

This model can estimate the variations of all the variables of the propulsion system during the burn time. By analysing the O/F ratio during combustion it is clear that the blowdown feeding system causes a non-negligible O/F ratio swift, this could reduce the performance and complicate the model description. To limit this phenomena a optimisation of the tanks volume and blowdown ratio has been performed.

### **3.4 Optimization of the initial conditions**

An optimization algorithm has been written to improve the performance and simultaneously reduce the overall mass and volumes, which are the most important parameters in every space propulsion design.

Since the model functions are pretty regular and continuous, a gradient method has been chosen with a single objective function to minimize.

#### **3.4.1 Variables, Constraint, Objective function**

The optimization variables chosen for this process are the blowdown ratio and the initial GHe volume inside each tank. The range of these variables has been chosen to maintain large freedom in tank sizes and being more restrictive for the blowdown ratio. This avoids unfeasible solutions, like a ratio lower than one.

The initial guesses of the optimization variables have been chosen as a set of random values inside the variable's ranges. The following optimization iterations, instead, used the results of the previous trial as initial guesses to improve convergence speed.

A non-linear set of inequalities have been imposed as constraints to obtain:

1. Final thrust target magnitude of 60N
2. Mass margin on fuel after burn time of 10%
3. Mass margin on oxidizer after burn time of 10%

The objective functions to minimize are a sum of three contributes: the first is the norm of the vector of absolute value of error in each time step of the blowdown simulation. This tells how much the O/F ratio

shifts from the ideal value during all the burn time. The other contributes are the two tanks volumes, which are minimized in order to reduce masses and system overall dimensions.

$$f(\vec{x}) = \sqrt{\sum |O\vec{F} - O/F_{opt}|} + V_{g_{fuel}} + V_{g_{ox}} \quad (3.2)$$

The weighting of these three contributions was roughly defined, anyway the results were very satisfying. A more advanced development could be carried out by studying a more accurate weighting method.

### 3.4.2 Optimization results

The best trial of optimization converged to a local minimum of the objective function respecting all the constraints and reached a maximum O/F ratio error of  $-1.08 \cdot 10^{-3}$ . Considering that the study done with NASA-CEA on the influence of the O/F ratio shift on the  $I_{sp}$  shows an maximum acceptable error in the order of 0.05, the results were better than the requirements of an order of magnitude.

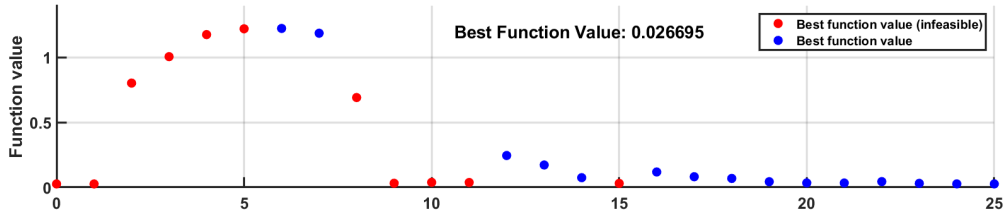


Figure 3.2: Iterations of the optimization function

The volumes of the tanks were also pretty acceptable compared to the solution with an adiabatic transformation, which were almost three times bigger than the isothermal values.

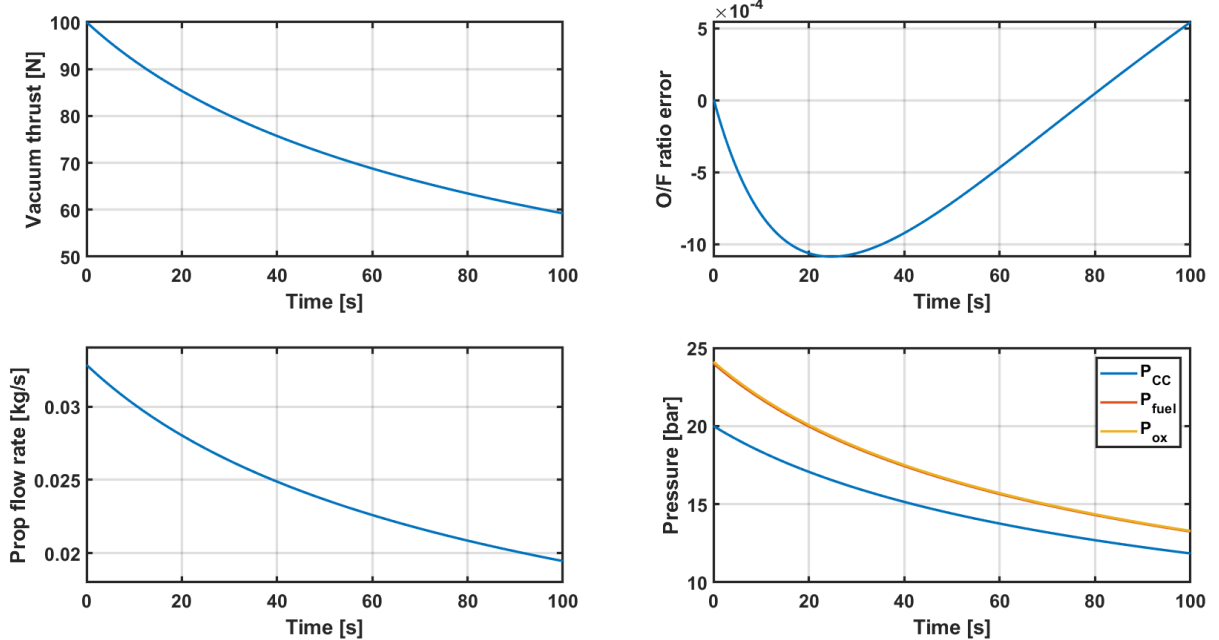


Figure 3.3: Results of the optimization

### 3.4.3 Detail of the numerical model and scripts

See App. E

# Chapter 4

## Statistical analysis

### 4.1 Montecarlo simulation

To properly investigate the variation of the performance parameters due to the natural production imperfections and existing uncertainties, it was decided to run a statistical analysis on the off-nominal firing of the engine, using the standard uncertainties (reduced to  $1\sigma$ ) of the most relevant input parameters used for the nominal simulation.

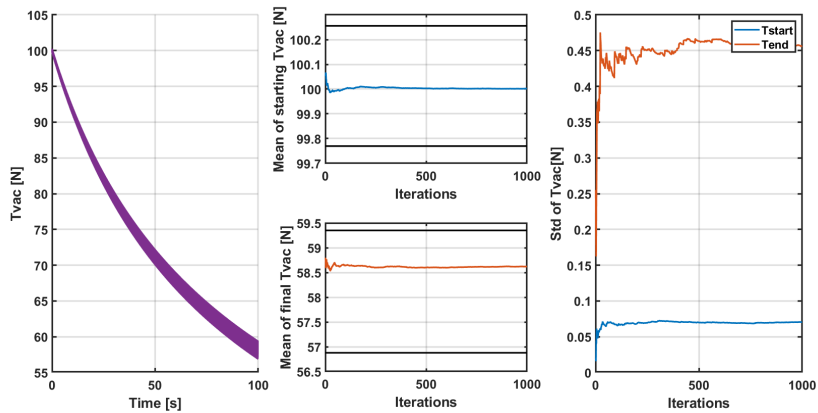


Figure 4.1: Results of Montercarlo simulation (black lines: max and min boundary values)

The most notable outputs of the simulation, the initial and final thrust, were then analyzed to determine if the system was robust enough. Clearly the initial and mostly the final thrust converge and variate in a minimal range, thus confirming that the system outputs respect the requirements (initial and final thrust, burning time) even in non-nominal conditions.

As expected, the final thrust has a more significant variation with respect to the initial one and to most of the uncertainties included in the model.

### 4.2 Determination of uncertainties

$D_t[m]$	$P_c[bar]$	$D_{FU}^{feed}[m]$	$D_{OX}^{feed}[m]$	$D_{FU}^{inj}[m]$	$D_{OX}^{inj}[m]$	$T_{amb}$	$\gamma_{poly}[-]$
$5.7681 \cdot 10^{-3}$	20	$4.7625 \cdot 10^{-3}$	$4.7625 \cdot 10^{-3}$	$3.7258 \cdot 10^{-4}$	$9.0260 \cdot 10^{-4}$	298.15	1

Table 4.1: Nominal values

$D_t[m]$	$P_c[bar]$	$D_{FU}^{feed}[m]$	$D_{OX}^{feed}[m]$	$D_{FU}^{inj}[m]$	$D_{OX}^{inj}[m]$	$T_{amb}$	$\gamma_{poly}[-]$
$2 \cdot 10^{-6}$	0.1	$10^{-4}$	$10^{-4}$	$10^{-6}$	$10^{-6}$	5	+0.033

Table 4.2: Standard deviation at  $1\sigma$

The nominal values are the ones calculated during the sizing (Chap. 2). The deviations were all connected to a Gaussian model with  $1\sigma$ . The uncertainties are directly correlated to the manufacturing

$D_t[m]$	$D_{FU}^{feed}[m]$	$D_{OX}^{feed}[m]$	$D_{FU}^{inj}[m]$	$D_{OX}^{inj}[m]$
$3.4674 \cdot 10^{-4}$	$2.12 \cdot 10^{-2}$	$2.1164 \cdot 10^{-2}$	$2.6840 \cdot 10^{-3}$	$1.1079 \cdot 10^{-3}$

Table 4.3: Relative standard variation of the design parameters

method that we have chosen (Chap. 5). The whole CC and nozzle is printed with additive manufacturing, while the feeding lines are made of drawn tubes. It was assumed that the ambient temperature could vary before the firing of the engine in a range of  $\pm 5K$ . The initial chamber pressure (a design requirement) was also considered in this analysis. The  $\pm 0.1bar$  variation was chosen to consider possible transients in the CC. To account for a possible variation of the isothermal expansion, it was also considered a range on the polytropic exponent that reduces its efficiency.

### 4.3 Sensitivity analysis

The OFAT (One Factor At a Time) method was used [9], with only the uncertainties related to the design considered in this process.

Active parameter	$D_t$	$D_{feed}$	$D^{inj}$
$\sigma_T^{end}[N]$	$3 \cdot 10^{-2}$	$1.4 \cdot 10^{-3}$	$10^{-2}$

Table 4.4: Std of final thrust with different uncertainties (App. F.3)

It can be seen that the uncertainty on the throat is the most stringent one, closely followed by the injectors and the feeding lines. Therefore a lot of attention must be paid to the production of those parts as they are the most critical ones.

### 4.4 Extension to 10N and 1000N thrusters

A preliminary conceptual analysis on the possible extension to 10N and 1000N while using the same engine configuration is presented in this section. The 1000N thruster should not give any issues since all the relative uncertainties would be lower and have less impact on the non-nominal performance. It could be built while scaling up proportionally the whole engine and keeping the same pressures in the tanks.

The 10N seemed more problematic: with the same configuration, the uncertainty related fluctuations could grow outside an acceptable range. This is mainly due to the sizing down of the engine, while the uncertainties dependant on the production methods remain the same.

Therefore, the relative uncertainties would be higher and the engine could suffer from drastically performance differences on each different engine produced (even if the nominal performance could be acceptable). Due to the latter consideration, the pressure friction losses would also considerably increase both in the feeding lines and in the CC. The isentropic approximation would not be accurate anymore. The downsizing of the injectors could also pose another problem as it would be difficult to manufacture a smaller one. This could be solved by changing the engine design, keeping the same geometry and size, and by lowering the chamber pressure to reduce the performance. Still, an in-depth analysis would be required to change configuration.

In conclusion, the upsizing to 1000N should not cause any problem while the downsizing to 10N would be hardly acceptable or even impossible without changing the overall design.

# Chapter 5

## Additive manufacturing

Inconel 718 alloy is a high-strength, corrosion-resistant nickel-chromium material widely used in the aerospace industry because of its ability to retain its mechanical properties at temperatures where other metals would show a significant decrement in performance. Its elevated hardness makes it also quite difficult to manufacture using common machinery; that's where 3D printing technology comes into play. It allows for the production of complex shapes at no extra cost as opposed to traditional production methods, but requires finishing and polishing. Among the wide choice of technologies available for printing, the one chosen was the Direct Metal Laser Sintering (DMLS) because it allows to produce objects with a better surface roughness if compared to other technologies and obtain a low porosity.

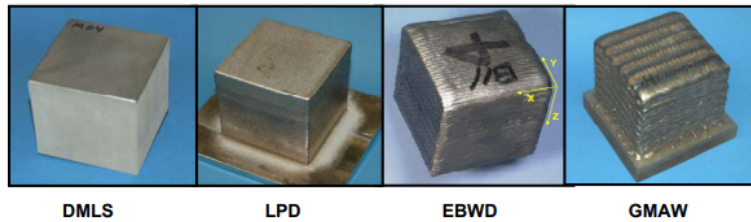


Figure 5.1: Shape-forming capability of different AM processes (DMLS=Direct Metal Laser Sintering, LPD=Laser Powder Deposition, EBWD=Electron Beam Wire Deposition, GMAW=Gas Metal Arc Welding) [10]

Parts produced using 3D printing technologies have an intrinsic high surface roughness compared to machined ones due to the thickness of the layers and the laser beam dimension. In order to increase its mechanical performance, Inconel 718 can be easily hardened by precipitation-hardening heat treatments. In both as-built and age-hardened states, the parts can be machined, spark-eroded using Electrical Discharge Machining (EDM) technology, micro shot-peened, polished and coated if required. [11]

After having acknowledged from literature [12] that the roughness obtainable with the DMLS manufacturing process is between 3.5 and 60  $\mu\text{m}$ , it was analysed the amount of total pressure losses with the Shapiro model (fig 2.3) assuming the highest possible roughness. The total pressure losses obtained is of 0.01%, so it was decided to not treat the internal surface of the combustion chamber with any machining or other processes.

This choice led to the possibility of 3D printing as a whole piece the injectors plate, the combustion chamber and the nozzle, exploiting the advantages of the manufacturing process and avoiding thermal and structural weaknesses. Since the diameter of the injectors is 0.3726 mm and 0.9026 mm for RP-1 and H<sub>2</sub>O<sub>2</sub> respectively, it's necessary to create the injector holes through an electro-erosion process after having 3D printed the injectors plate. Moreover, to improve the roughness of the internal surface of the divergent part of the nozzle it was decided to treat it with an electrochemical polishing process obtaining a final roughness up to 1.5  $\mu\text{m}$  [13].

# Bibliography

- [1] Lecture slides, *Space Propulsion, F. Maggi.*
- [2] Karthik Venkatesh Mani, Francesco Topputo, Angelo Cervone, *Chemical Propulsion System Design for a 16U Interplanetary CubeSat*, IAC-18-C4.6.2.x47764.
- [3] K.N.C. Bray. *Simplified sudden-freezing analysis for non-equilibrium nozzle flows*. ARS Journal, pages 831—834, 1961.
- [4] G.P. Sutton, O. Biblarz, *Rocket Propulsion Elements*, John Wiley & Sons, Inc., 2001.
- [5] *Rocket Propulsion Analysis*, <https://www.rocket-propulsion.com/index.htm>.
- [6] INCONEL alloy 718 (UNS N07718/W.Nr. 2.4668), [www.specialmetals.com](http://www.specialmetals.com).
- [7] Eric J. Wernimont, Mark C. Ventura, Mark C. Grubelich, Mark R. Vaughn, William R. Escapule, *Low Temperature Operation of Hydrogen Peroxide Gas Generators: Verification Testing & Possible Applications*, AIAA 2009-4617, 2 - 5 August 2009, Denver, Colorado.
- [8] *Technical Hydraulic Handbook*, 12th Edition, The Lee Company Technical Center, Westbrook, Connecticut 06498-0424 U.S.A.
- [9] Czitrom, Veronica (1999). "One-Factor-at-a-Time Versus Designed Experiments". *American Statistician*. 53 (2): 126–131. doi:10.2307/2685731. JSTOR 2685731.
- [10] Raymond C. Benn & Randy P. Salva, *Additively Manufactured Inconel Alloy 718*, Materials and Process Engineering, Pratt & Whitney, 400 Main Street, E. Hartford, CT 06108 .
- [11] Material data sheet, *EOS NickelAlloy IN718*.
- [12] *Considerations for Optimizing Surface Finishing of 3D Printed Inconel 718*, PostProcess Technologies, Inc., 2019.
- [13] Srishti J., Mike C., Bruce T., and Wayne N. H., *Electrochemical polishing of selective laser melted Inconel 718*, 47th SME North American Manufacturing Research Conference, NAMRC 47, Pennsylvania, USA.
- [14] B. Boust, J.-B. Lebon, M. Bellenoue, A. Tran, R. Beauchet, Y. Batonneau, É. Labarthe and Y. Guélou, *Catalytic Ignition of Hydrogen Peroxide for Storable Bipropellant Thrusters*, doi:10.13009/EUCASS2019-944.
- [15] G.F. Froment, K.C. Waugh, *Reaction Kinetics And The Development And Operation of Catalytic Processes*, 2001 ELSEVIER.
- [16] Chemical and Material Sciences Department, Research Division - Rocketdyne, a Division of North American Aviation, Inc. Canoga Park, California, *Hydrogen Peroxide Handbook*, July 1967.
- [17] Eric J Wernimont and Dick Durant, *Development of a 250 lbfv Kerosene – 90% Hydrogen Peroxide Thruster*, AIAA 2004-4148, 11 - 14 July 2004, Fort Lauderdale, Florida.
- [18] R. J. Kuntz, PE, R. G. Sjogren, *Advanced Propellant Staged-Combustion Feasibility Program*, Aerojet-General Corporation, September 1967.
- [19] Eric J Wernimont, *Hydrogen Peroxide Catalyst Beds: Lighter and Better Than Liquid Injectors*, AIAA-2005-4455, Tucson, AZ, July 10-13, 2005.

- [20] MATLAB:R2022a, Natick, Massachusetts, The Mathworks, Inc., MATLAB version 9.12.0.1884302 (R2022a), 2022.
- [21] S. Gordon and B. J. McBride, "Computer Program for Calculation of Complex Chemical Equilibrium Compositions and Applications," NASA Reference Publication 1311 (1996).

# Appendix A

## CAD modelling



Figure A.1: Total CAD model of the designed propulsion system

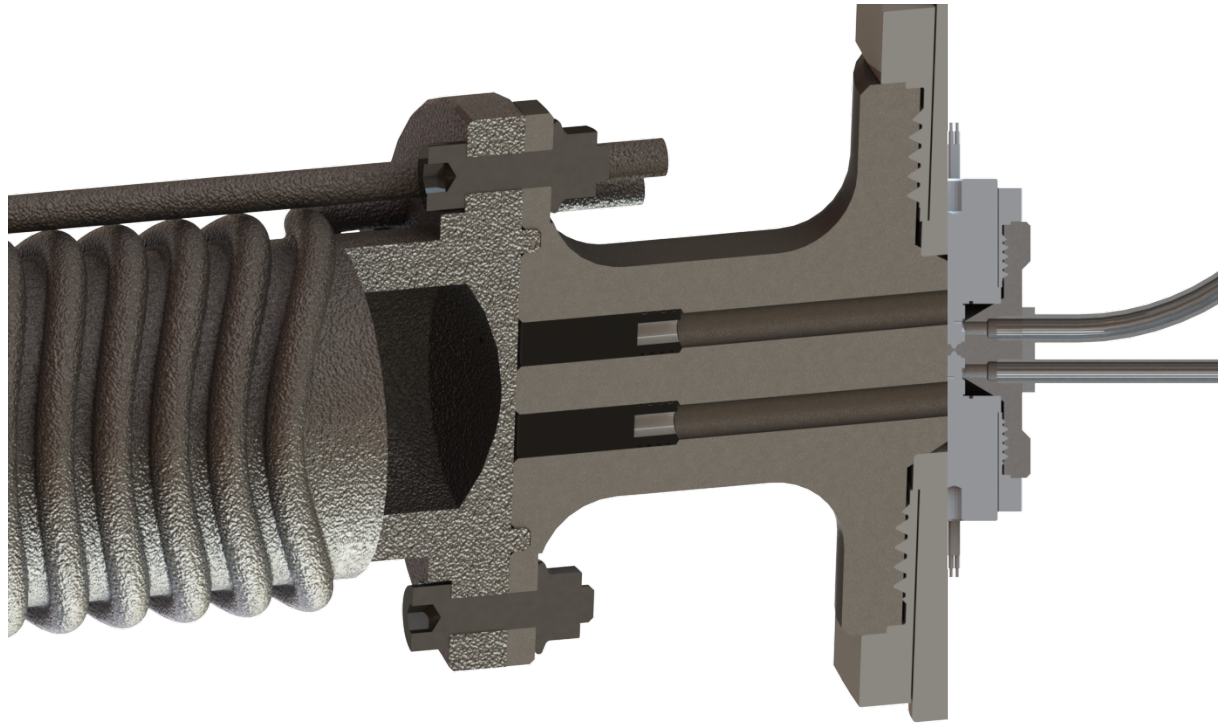


Figure A.2: Cut-off view of AM injector plate design

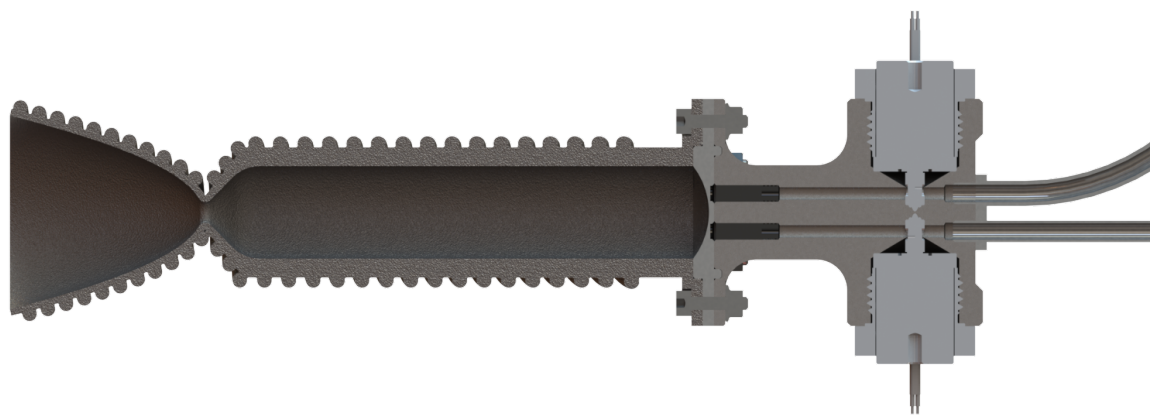


Figure A.3: Cut-off view of separate injector plate design

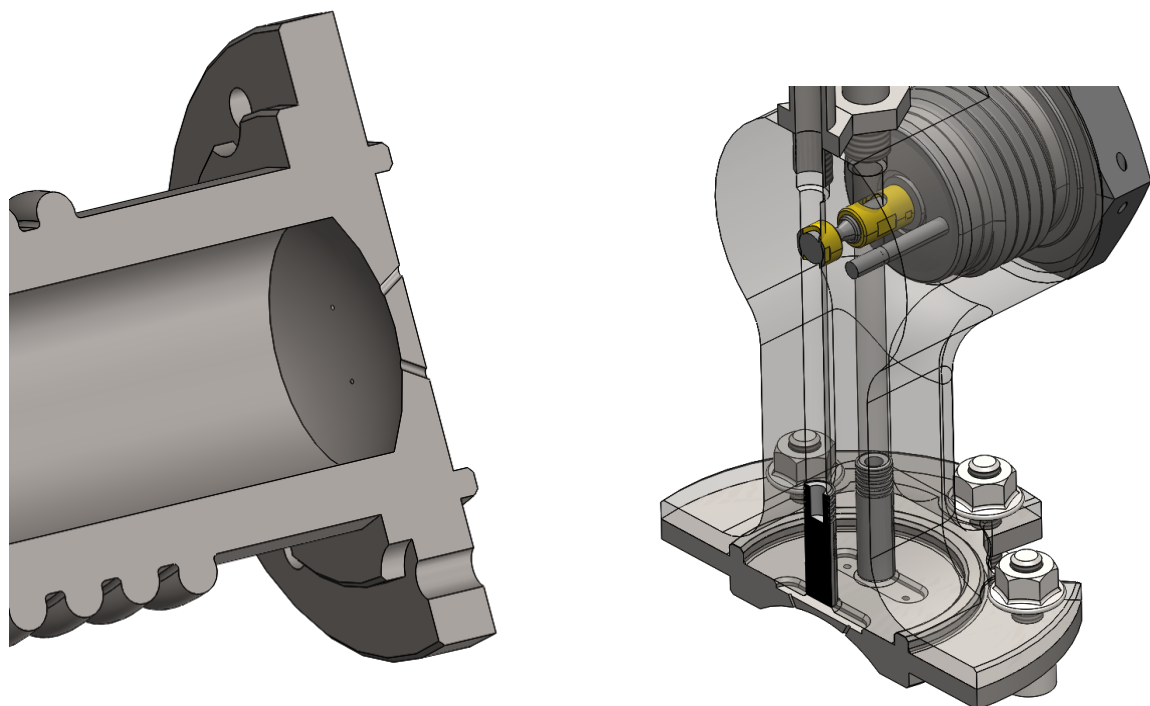


Figure A.4: Injector design

## Appendix B

# Literature review of injection and combustion with liquid H<sub>2</sub>O<sub>2</sub>

Traditionally, in the cases when hydrogen peroxide is selected as an oxidizer, there have been two general methods of obtaining combustion with a fuel[14]. The first method is to decompose the hydrogen peroxide in a catalyst bed, and then fuel is sprayed into the catalyst exhaust products [15]. This process is referred to in literature as staged combustion, and for most fuels, the H<sub>2</sub>O<sub>2</sub> decomposed products spontaneously ignite the propellant. Hence, in the combustion chamber, no separate igniter is required and the liquid fuel is injected into a gaseous superheated steam of H<sub>2</sub>O<sub>2</sub> [16]. The second method, called liquid-liquid injection, is to co-inject liquid hydrogen peroxide with liquid fuel. In order to achieve combustion, a catalyst can be used to make the propellant couple hypergolic and permit auto-ignition, although it is possible to ignite the mixture by a separate device.

The catalyst bed based system (staged combustion) is superior to the liquid-liquid injection based system in three significant aspects:

1. Reliability and safety: it is less prone to hard starts during ignition and more deterministic in operation. In other words, it allows for a smoother ignition, while the liquid-liquid injection based system suffers from some high-pressure spikes during ignition. In fact, experimental data has shown that ignition times of 20 ms have been achieved with a staged combustion system, using 90% H<sub>2</sub>O<sub>2</sub> and RP-1 [17].
2. Performance: the staged combustion-based system produces higher combustion efficiency for shorter L\*. Thus, it requires less combustion chamber mass (because it is faster) for the same combustion efficiency level. Therefore the use of gas-on-liquid injection, which results from catalytic staged combustion, provides for better mixing and combustion efficiency for a given L\* [18].
3. Reduced powerhead mass: given the state of the art in catalyst bed technology, the staged combustion system provides for a lighter system by a factor of 2.5, which can increase to over 3.5 if higher chamber pressures and higher fluxes are used [19].

Concerning the specific couple used for the propulsive unit analysed, Rocket Propellant 1 (RP-1) is a storable rocket fuel used in the industry for its safety in handling, low price and density if compared to liquid hydrogen, which, on the other hand, provides a higher I<sub>sp</sub>. Its low vapour pressure provides a safe environment for ground crews but negates the ability to self-pressurize.

One upside of RP-1 combustion is the formation of soot below 70bar pressure, which acts as an insulation layer by adhering to the surfaces of the combustion chamber and nozzle. In this way it reduces the heat flow to the walls by roughly a factor of 2, which makes up for the low thermal conductivity of Inconel 718. Hydrogen Peroxide (H<sub>2</sub>O<sub>2</sub>) is also a storable liquid that requires simple handling precautions, which provides high specific energy release.

## Appendix C

# Preliminary analysis

### C.1 Tables and graphs

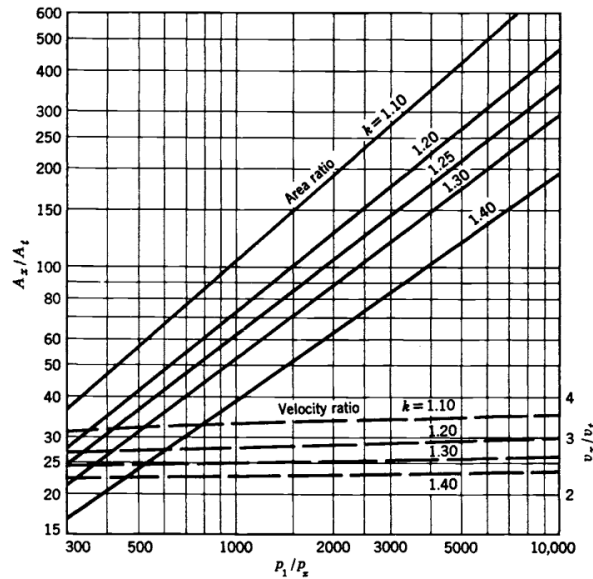


Figure C.1: Area and velocity ratios as function of pressure ratio for the diverging section of a supersonic nozzle.

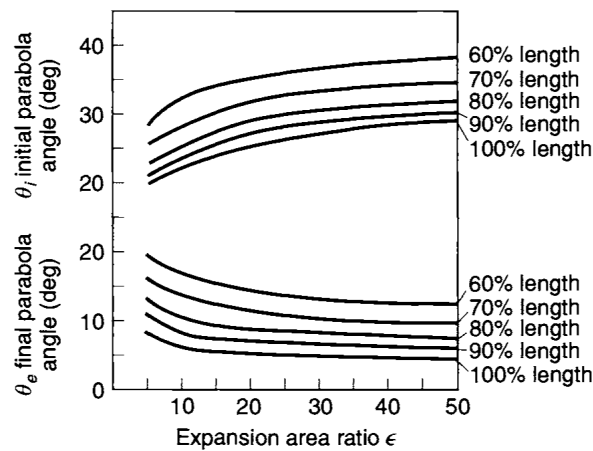


Figure C.2: Parabola angles as function of expansion ratio.

Oxidizer	Fuel	Mixture Ratio		Average Specific Gravity	Chamber Temp. (K)	Chamber $c^*$ (m/sec)	$M_{mol}$ (g/mol)	$I_x$ (sec)		$k$
		By Mass	By Volume					Shifting	Frozen	
Oxygen	Methane	3.20	1.19	0.81	3526	1835			296	
		3.00	1.11	0.80	3526	1853		311		
	Hydrazine	0.74	0.66	1.06	3285	1871	18.3		301	1.25
		0.90	0.80	1.07	3404	1892	19.3	313		
	Hydrogen	3.40	0.21	0.26	2959	2428	8.9		386	1.26
		4.02	0.25	0.28	2999	2432	10.0	389.5		
	RP-1	2.24	1.59	1.01	3571	1774	21.9	285.4		1.24
		2.56	1.82	1.02	3677	1800	23.3		300	
	UDMH	1.39	0.96	0.96	3542	1835	19.8		295	1.25
		1.65	1.14	0.98	3594	1864	21.3	310		
Fluorine	Hydrazine	1.83	1.22	1.29	4553	2128	18.5	334		1.33
		2.30	1.54	1.31	4713	2208	19.4		365	
	Hydrogen	4.54	0.21	0.33	3080	2534	8.9		389	1.33
		7.60	0.35	0.45	3900	2549	11.8	410		
	Hydrazine	1.08	0.75	1.20	3258	1765	19.5		283	1.26
Nitrogen tetroxide		1.34	0.93	1.22	3152	1782	20.9	292		
	50% UDMH-	1.62	1.01	1.18	3242	1652	21.0		278	1.24
	50% hydrazine	2.00	1.24	1.21	3372	1711	22.6	289		
	RP-1	3.4	1.05	1.23	3290		24.1		297	1.23
	MMH	2.15	1.30	1.20	3396	1747	22.3	289		
Red fuming nitric acid		1.65	1.00	1.16	3200	1591	21.7		278	1.23
	RP-1	4.1	2.12	1.35	3175	1594	24.6		258	1.22
		4.8	2.48	1.33	3230	1609	25.8	269		
	50% UDMH-	1.73	1.00	1.23	2997	1682	20.6		272	1.22
Hydrogen peroxide (90%)	50% hydrazine	2.20	1.26	1.27	3172	1701	22.4	279		
	RP-1	7.0	4.01	1.29	2760		21.7		297	1.19

Notes:

Combustion chamber pressure—1000 psia (6895 kN/m<sup>2</sup>); nozzle exit pressure—14.7 psia (1 atm); optimum expansion.

Adiabatic combustion and isentropic expansion of ideal gas

The specific gravity at the boiling point was used for those oxidizers or fuels that boil below 20°C at 1 atm pressure.

Mixture ratios are for approximate maximum value of  $I_x$ .

Figure C.3: Theoretical Performance of Liquid Rocket Propellant Combinations

## C.2 Nozzle and chamber geometry calculation

### C.2.1 Main equations

$$c^* = \frac{P_c \cdot A_t}{\dot{m}} = \frac{\sqrt{\frac{R_u \cdot T_c}{M_m}}}{\sqrt{\gamma \left( \frac{2}{\gamma+1} \right)^{\frac{\gamma+1}{\gamma-1}}}} \quad (C.1)$$

$$c_t = \frac{T}{P_c \cdot A_t} = \sqrt{\frac{2\gamma^2}{\gamma-1} \left( \frac{2}{\gamma-1} \right)^{\frac{\gamma+1}{\gamma-1}} \left[ 1 - \left( \frac{P_e}{P_c} \right)^{\frac{\gamma-1}{\gamma}} \right]} + \frac{P_e}{P_c} \cdot \epsilon \quad (C.2)$$

### C.2.2 Matlab script

```

1 %% STARTER
2 clear
3 close all
4 clc
5
6 %CEA data
7 Pe_CEA=0.01589e5;
8 Is_CEA = 312.7371;
9 OF = 7.5;
10 k=1.2083;
11 %k = 1.138;
12
13 %Mass flow rates
14 % T_nominal = 100;
15 % g0 = 9.81;
16 % m_dot = T_nominal/(Is_CEA*g0);
17 % m_dot_OX = (OF/(1+OF))*m_dot;
18 % m_dot_F = m_dot - m_dot_OX;
19
20 %% THROAT AREA AND EXTERNAL AREA SIZING
21
22 %k = 1.19; %FIRST K ITERATION: from table 5-5 pag 8 file Useful-Tables-V02
23 %Pe_Pc with graphical method = 0.00085 (from graphic slide 27 file ...
    02-Non-reacting-flows-2022-V01)

```

```

24
25 Pe_Pc = 0.00083767; %found by iterating the ratio Pe/Pc in the following equation to ...
26     have eps = 80
27 %Pe_Pc = 0.001152165;
28 eps=(((k+1)/2)^(1/(k-1))*(Pe_Pc^(1/k))*sqrt( ((k+1)/(k-1))*(1-(Pe_Pc^((k-1)/k)))) )^(-1);
29
30 Pc=20e5; % [Pa], requirement of the problem
31 Pe=Pe_Pc*Pc;
32 Pa=0; %expansion in vacuum
33 cF=sqrt(2*(k^2)/(k-1)*((2/(k+1))^( (k+1)/(k-1)))*(1-(Pe_Pc)^((k-1)/k)))+((Pe-Pa)/Pc)*eps;
34
35 %1D thrust to have 2D thrust of 100 N
36 Tconic=101.7332;%Thrust corrected considering the losses due to divergence (conic nozzle)
37 TRAO1=102.5892;%Thrust corrected considering the losses due to divergence (RAO minimum ...
38 length nozzle)
39 TRAO2=100.7088;%Thrust corrected considering the losses due to divergence (RAO maximum ...
40 performance nozzle)
41
42 At=TRA02/(Pc*cF);%m^2
43 Dt=sqrt(4*At/pi);%m
44 Ae=eps*At;
45 De=sqrt(4*Ae/pi);
46
47 %% #1 CONIC NOZZLE:
48
49 alpha=15;% [deg]
50 Ldiv_conic=(De-Dt)/(2*tan(deg2rad(alpha)));
51 beta=45;%reason: in the convergent you have a positive pressure gradient and low speed ...
52 so you can afford a greater angle, to have a shorter convergent length, without ...
53 impacting the fluid dynamics
54
55 lambda_conic=(1+cos(deg2rad(alpha))/2;
56 T2D_conic=Tconic*lambda_conic;
57
58 % OPTION 1: Assumed Mach in combustion chamber of 0.3
59
60 Mc1_conic=0.3;%assumed ranging between 0.2 and 0.4
61 Ac1_conic=(At/Mc1_conic)*((2/(k+1))*(1+((k-1)/2)*(Mc1_conic^2)))^((k+1)/(2*(k-1)));
62 Dc1_conic=sqrt(4*Ac1_conic/pi);
63 Lc1_conic=((Dc1_conic-Dt)/2)/tan(deg2rad(beta));
64 Ltot1_conic=Lc1_conic+Ldiv_conic;
65 Ac_At_1 = Ac1_conic/At;
66
67 % OPTION 2: contraction ratio assumed of 6
68
69 Ac_At_2 = 18;%assumed from slide number 13 file liquid-part2
70 Ac2_conic= Ac_At_2 * At;
71 Dc2_conic=sqrt(4*Ac2_conic/pi);
72 fun=@(Mc2_conic) ...
73     (At/Mc2_conic)*((2/(k+1))*(1+((k-1)/2)*(Mc2_conic^2)))^((k+1)/(2*(k-1))-Ac2_conic);
74 opt=optimset('Display','Off');
75 Mc2_conic=fzero(fun,0.3,opt);
76 Lc2_conic=((Dc2_conic-Dt)/2)/tan(deg2rad(beta));
77 Ltot2_conic=Lc2_conic+Ldiv_conic;
78
79 % CHECK with mass flow conservation for Mc verification:
80
81 % rho_c = 1.9502; % kg/m^3
82 % rho_t = 1.2007;
83 % a_c = sqrt(k*8.314/21.695*2675.99);
84 % a_t = sqrt(k*8.314/21.825*2517.97)
85 %
86 % M = (rho_t.*a_t) ./ ([3:1:6].*rho_c.*a_c)
87
88 %% #2 RAO NOZZLE:
89
90 Ldiv_RAO=Ldiv_conic;
91
92 % #1 MINIMUM LENGTH APPROACH:
93
94 Ldiv_RAO1=0.6*Ldiv_RAO;
95 tetail=38.5;% deg from RAO graphic curves

```

```

91 tetael=12.5;% deg from RAO graphic curves
92 alphal=rad2deg(atan((De-Dt)/(2*Ldiv.RAO1)));
93 lambda1.RAO=0.5*(1+cos(deg2rad((alphal+tetael)/2)));
94 T2D.RAO1=lambda1.RAO*TRA01;
95 Ltot1.RAO1=Ldiv.RAO1+Lc1.conic; %with M=0.3 see 29 row
96 Ltot1.RAO2=Ldiv.RAO1+Lc2.conic; %with M=0.2020 see 35 row
97
98 % #2 MAXIMUM PERFORMANCE APPROACH:
99
100 Ldiv.RAO2=1*Ldiv.RAO;
101 tetai2=31;%deg from RAO graphic curves
102 tetae2=4.25;%deg from RAO graphic curves
103 alpha2=rad2deg(atan((De-Dt)/(2*Ldiv.RAO2)));
104 lambda2.RAO=0.5*(1+cos(deg2rad((alpha2+tetae2)/2)));
105 T2D.RAO2=lambda2.RAO*TRA02;
106 Ltot2.RAO1=Ldiv.RAO2+Lc1.conic; %with M=0.3 see 29 row
107 Ltot2.RAO2=Ldiv.RAO2+Lc2.conic; %with M=0.2020 see 35 row
108
109 %% FINAL DATA
110
111 format long
112 Area_C = Ac2.conic
113 Diam_C = Dc2.conic
114 Area_E = Ae
115 Diam_E = De
116 Area_T = At
117 Diam_T = Dt
118 Lunghezza_conv = Lc2.conic
119 Lunghezza_div = Ldiv.RAO2
120 Lunghezza_tot = Lunghezza_conv + Lunghezza_div
121
122 %% Combustion Chamber Sizing
123
124 L_chr=1.2*1.778; % [m]
125 rho_c=1.9502; %[kg/m^3]
126 theta=45; % deg
127 c_chr=1591.7; %m/s
128 Ac_At_2=18;
129
130 V_c=L_chr*Area_T; %[m^3]
131 m_p=Pc*Area_T/c_chr; %[kg/s]
132 t_res=L_chr/m_p*rho_c*Area_T; %[s]
133
134 Lunghezza_CC=(V_c/Area_T-1/3*sqrt(Area_T/pi)*cot(deg2rad(theta))*(Ac_At_2^(1/3)-1))/Ac_At_2 ... % [m]
135
136 %% Data Export
137 nozzle_variables=[Area_T c_chr OF Pc cF lambda2.RAO];
138 save('nozzle_variables.mat','nozzle_variables');

```

### C.3 CEA analysis

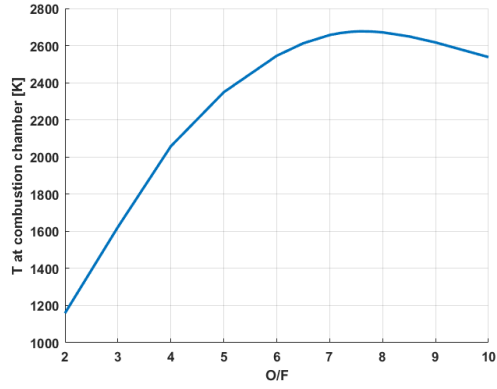


Figure C.4: Combustion chamber temperature

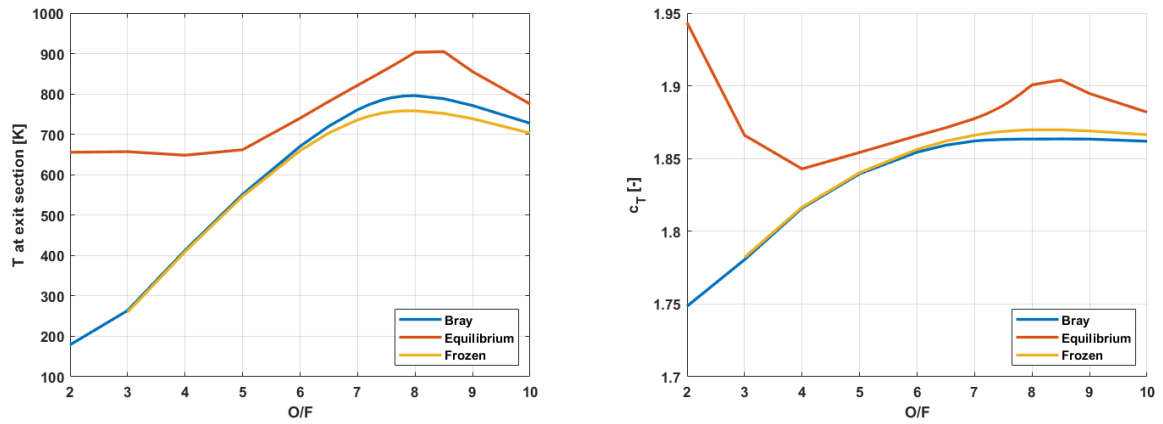


Figure C.5: Exit temperature and Thrust coefficient

Figure C.6: CEA analysis

### C.3.1 Optimal NASA-CEA analysis

```

1 THEORETICAL ROCKET PERFORMANCE ASSUMING FROZEN COMPOSITION
2 AFTER POINT 2
3
4 Pin = 290.1 PSIA
5 CASE = CEA_PROP
6
7          REACTANT           WT FRACTION      ENERGY      TEMP
8                               (SEE NOTE)      KJ/KG-MOL      K
9 OXIDANT      H2O2(L)        0.8750000   -187780.000   298.150
10 OXIDANT     H2O(L)         0.1250000   -285830.088   298.150
11 FUEL        RP-1           1.0000000   -24717.700   298.150
12
13 O/F=    7.50000  %FUEL= 11.764706 R,EQ.RATIO= 1.045514 PHI,EQ.RATIO= 1.103305
14
15          CHAMBER      THROAT      EXIT
16 Pin/P      1.0000    1.7365   1258.49
17 P, BAR     20.000    11.518   0.01589
18 T, K       2675.99   2517.97   787.60
19 RHO, KG/CU M 1.9502 0 1.2007 0 5.2965-3
20 H, KJ/KG   -6220.19  -6767.79  -10617.4
21 U, KJ/KG   -7245.74  -7727.05  -10917.4
22 G, KJ/KG   -38982.5  -37595.4  -20260.0
23 S, KJ/(KG) (K) 12.2431 12.2431 12.2431
24
25 M, (1/n)    21.695   21.825   21.825
26 MW, MOL WT 21.695   21.825   21.825
27 Cp, KJ/(KG) (K) 4.2633  3.7277  1.8274
28 GAMMAs     1.1346   1.1418   1.2634
29 SON VEL, M/SEC 1078.7  1046.5  615.7
30 MACH NUMBER 0.000    1.000    4.817
31
32 PERFORMANCE PARAMETERS
33
34 Ae/At      1.0000   80.000
35 CSTAR, M/SEC 1591.7  1591.7
36 CF          0.6575   1.8631
37 Ivac, M/SEC 1963.1  3066.7
38 Isp, M/SEC  1046.5  2965.5
39
40 MOLE FRACTIONS
41
42 *CO         0.03335  *CO2        0.15036  *H        0.00133
43 *H2         0.02755  H2O        0.77554  *O        0.00025
44 *OH         0.00873  *O2        0.00288
45
46 * THERMODYNAMIC PROPERTIES FITTED TO 20000.K
47
48 NOTE. WEIGHT FRACTION OF FUEL IN TOTAL FUELS AND OF OXIDANT IN TOTAL OXIDANTS

```

## Appendix D

### Thermal analysis

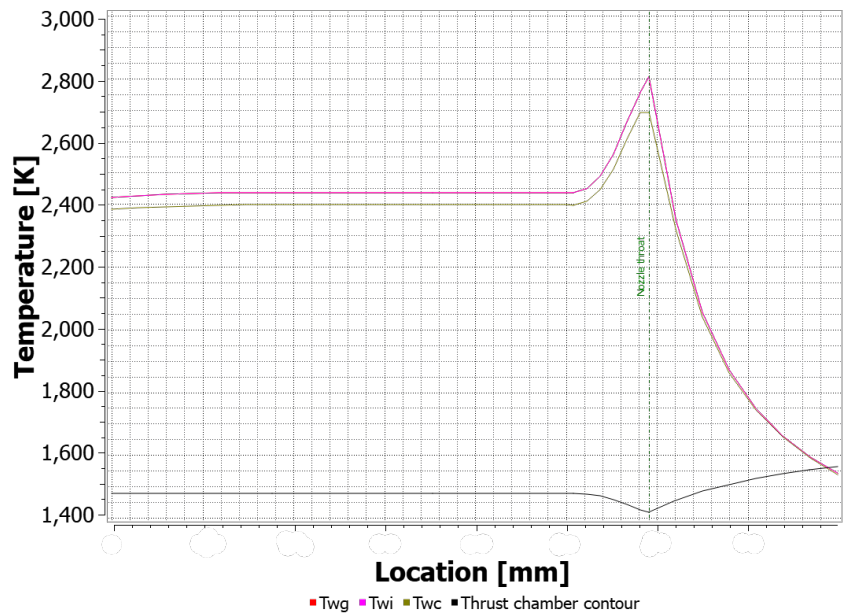


Figure D.1: Wall temperatures with radiative cooling

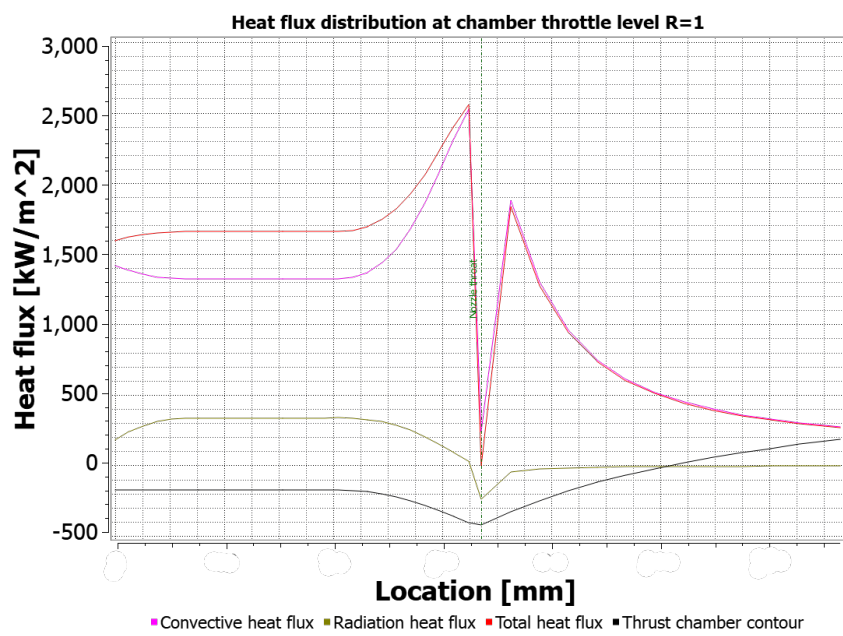


Figure D.2: Heat transfer with radiative cooling

# Appendix E

## Blowdown model

### E.1 Pressure losses estimation

#### E.1.1 Equations

$$K_{dist} = \frac{8 \cdot \lambda_{dist} \cdot L}{\pi^2 \cdot D^5 \cdot \rho} \quad (\text{E.1})$$

$$K_{conc} = \frac{\Delta P}{\dot{m}^2} \quad (\text{E.2})$$

#### E.1.2 Figures and Matlab function

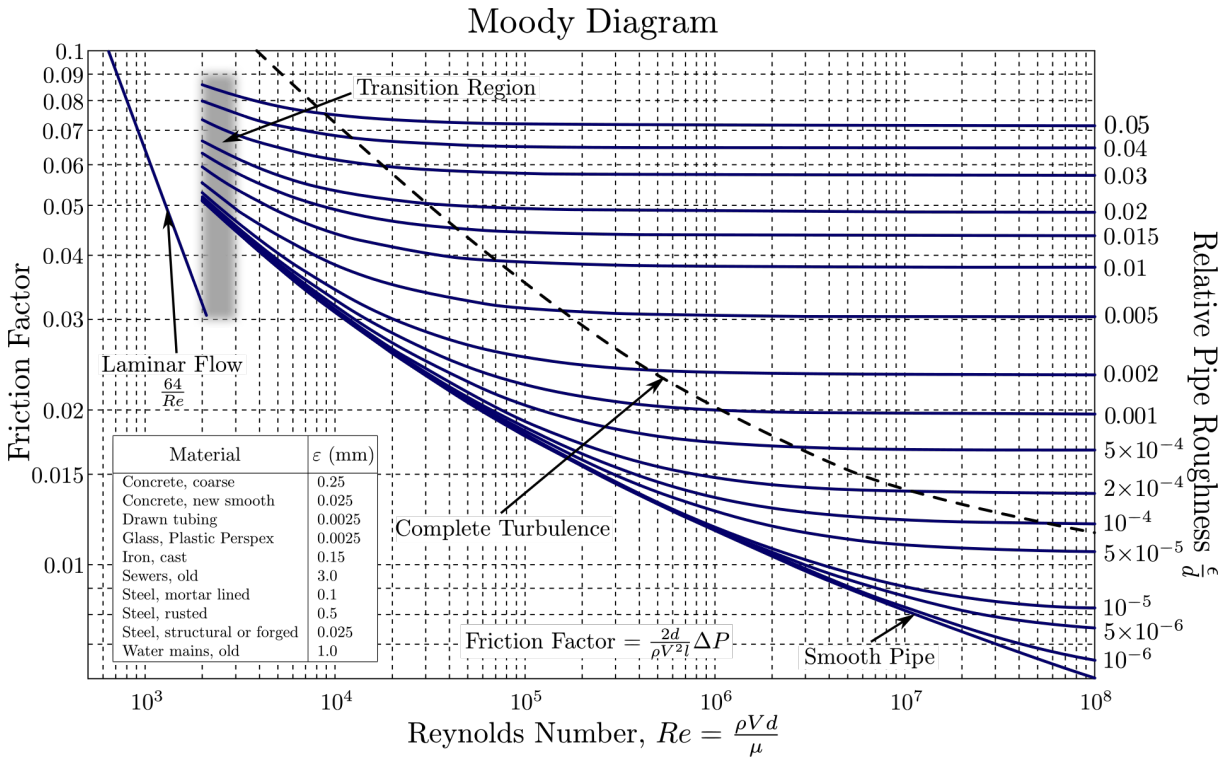


Figure E.1: Moody diagram

A Matlab function has been developed to obtain the overall pressure loss coefficient on fuel and oxidizer feeding lines. To get the total parameters have been considered the injector, check valves, latch valves and the distributed losses along the pipelines. To obtain the lambda coeff. of friction for the distributed losses the Reynolds number is computed and a laminar model of friction has been described. If Reynolds is lower than 2000 the laminar model compute automatically the lambda coeff., otherwise a turbulent model was applied and the lambda value must be obtained graphically from Moody diagram.

```

1 function [K1,K2] = K_estim (Qm,Pc,OF,d1,d2,dj1,dj2)
2
3 % -----
4 % Input:
5 % Qm Mass flow rate nominal [kg/s]
6 % Pc CC Pressure [Pa]
7 % OF Ox-Fuel ratio
8 % d1 Fuel tubing diameter [m]
9 % d2 Ox tubing diameter [m]
10 % dj1 Fuel injector diameter [m]
11 % dj2 Ox injector diameter [m]
12 %
13 % Output:
14 % K1 Fuel tubing line losses coeff.
15 % K2 Ox tubing line losses coeff.
16 % -----
17
18 L1 = 0.200; % Length Tank-Latch-Valve [m]
19 rough = 0.0024e-3; % Roughness [m] drawn tube
20 R_f = rough/d1; % Fuel relative roughness
21 R_ox = rough/d2; % Ox relative roughness
22 rho_f = 800.96; % Fuel density [kg/m^3]
23 rho_ox = 1308; % Ox density [kg/m^3]
24 mu_f = 1.743e-3; % Fuel viscosity @293.15K [Pa*s]
25 mu_ox = 1.249e-3; % Ox viscosity @293.15K [Pa*s]
26 Cd = 0.7; % Injector discharge coeff.
27
28 Qm_f = Qm*(1/(OF+1)); % Fuel mass flow rate [kg/s]
29 Qm_ox = Qm*(OF/(OF+1)); % Ox mass flow rate [kg/s]
30 Q_f = Qm_f/rho_f; % Fuel flow rate [m^3/s]
31 Q_ox = Qm_ox/rho_ox; % Ox flow rate [m^3/s]
32 u_f = Q_f/(d1^2*pi/4); % Fuel velocity [m/s]
33 u_ox = Q_ox/(d2^2*pi/4); % Ox velocity [m/s]
34
35 Re_f = rho_f/mu_f*d1*u_f; % Reynolds number in fuel pipe
36 if Re_f<2000
37 % fprintf('Fuel -> laminar flow: Re=%f \n',Re_f);
38 lambda_f=64/Re_f; % Fuel Darcy friction factor
39 else
40 % fprintf('!! Warning !! Fuel -> turbulent flow: Re=%f \nRelative roughness: ...
41 %d \nEvaluate manually lambda\n', Re_f, R_f);
42 lambda_f=0.045; % Fuel Darcy friction factor from moody diagram
43 end
44
45 Re_ox = rho_ox/mu_ox*d2*u_ox; % Reynolds number in ox pipe
46 if Re_ox<2000
47 % fprintf('Oxidizer -> laminar flow: Re=%f \n',Re_ox);
48 lambda_ox=64/Re_ox; % Ox Darcy friction factor
49 else
50 % fprintf('!! Warning !! Oxidizer -> turbulent flow\nRe=%f \nRelative roughness: ...
51 %d\nevaluate manually lambda\n', Re_ox, R_ox);
52 lambda_ox=0.038; % Ox Darcy friction factor from moody diagram
53 end
54
55 K_L1_f = 8*lambda_f*L1/pi^2/d1^5/rho_f; % Distributed fuel losses coeff.
56 K_L1_ox = 8*lambda_ox*L1/pi^2/d2^5/rho_ox; % Distributed ox losses coeff.
57 K_V2 = 1.7322e6; % 3DCSFA1876-05A Check Valve ...
58 % losses coeff.
59 K_V1 = 8.6610e6; % SDLA2121033B Solenoid Valve ...
60 % loss coeff.
61 K_inj_1 = 2/(rho_f*Cd^2*dj1^4*pi^2); % Fuel injector losses
62 K_inj_2 = 2/(rho_ox*Cd^2*dj2^4*pi^2); % Ox injector losses
63 P_f = (Pc + 1/2*rho_f*u_f^2 + (K_L1_f +K_V1 +K_V2+K_inj_1)*Qm_f^2); % Fuel Tank ...
64 % Initial Pressure [Pa]
65 P_ox = (Pc + 1/2*rho_ox*u_ox^2 + (K_L1_ox+K_V1 +K_V2+K_inj_2)*Qm_ox^2); % Oxidizer Tank ...
66 % Initial Pressure [Pa]
67
68 K1 = (P_f-Pc)/Qm_f^2; % Total Fuel pressure losses coeff.[1/kg*m]
69 K2 = (P_ox-Pc)/Qm_ox^2; % Total Ox pressure losses coeff. [1/kg*m]

```

## E.2 Blowdown analysis

### E.2.1 Mathematical equations and discretized model

$$\dot{m}^{[i]} = \frac{P_{gas}^{[i]} \cdot A_t}{c^*} \quad (\text{E.3})$$

$$M_{prop}^{[i+1]} = M^{[i]} - \Delta t \cdot \dot{m}^{[i]} \quad (\text{E.4})$$

$$V_{prop}^{[i+1]} = M_{prop}^{[i+1]} \cdot \rho_{prop} \quad (\text{E.5})$$

$$V_{gas}^{[i+1]} = V_{gas}^{[i]} + V_{prop}^{[i]} - V_{prop}^{[i+1]} \quad (\text{E.6})$$

$$T_{gas}^{[i+1]} = T_{gas}^{[i]} \left( \frac{V_{gas}^{[i]}}{V_{gas}^{[i+1]}} \right)^{\gamma-1} \quad (\text{E.7})$$

$$P_{gas}^{[i+1]} = P_{gas}^{[i]} \left( \frac{V_{gas}^{[i]}}{V_{gas}^{[i+1]}} \right)^\gamma \quad (\text{E.8})$$

$$\begin{cases} \dot{m}_{fuel} = \sqrt{\frac{P_{fuel} - P_c}{K_{fuel}}} \\ \dot{m}_{ox} = \sqrt{\frac{P_{ox} - P_c}{K_{ox}}} \\ P_c = \frac{(\dot{m}_{fuel} + \dot{m}_{ox}) \cdot c^*}{A_t} \end{cases} \quad (\text{E.9})$$

$$O/F = \frac{\dot{m}_{ox}}{\dot{m}_{fuel}} \quad (\text{E.10})$$

$$T = P_c \cdot c_t \cdot A_t \cdot \lambda_{RAO_{2D}} \quad (\text{E.11})$$

### E.2.2 Matlab script

This script launches the nozzle script to obtain the geometry data of the nozzle and the performance coeff. to estimate the thrust over time. Could be also customized varing the gamma coeff. of the polytropic transformation of the gas to obtain a complete range of transformations if the cooling system would not be able to achieve a correct temperature management of the tanks guaranteeing a correct isothermal tranformation.

The above reported set of equations are iterated over time to reach a complete simulation of the behaviour of the propulsion system.

Terminated the blowdown simulation the thrust vector could be evaluated and the volume of tanks has been sized.

```

1 s1_nozzle;
2 clear
3 clc
4 close all
5 format short
6
7 %% Variables
8
9 %----- Variables from Optimization -----
10 B=1.9048; % Blowdown ratio [-]
11 Vg1(1) = 0.00044221; % He Fuel tank initial volume [m^3]
12 Vg2(1) = 0.0020233 ; % He Ox tank initial volume [m^3]
13 %
14
15 nozzle_variables = load('nozzle_variables.mat','nozzle_variables');
16 At = nozzle_variables.nozzle_variables(1); % Throat area [m^2]
17 cstar = nozzle_variables.nozzle_variables(2); % C* [m/s]
18 OFratio(1) = nozzle_variables.nozzle_variables(3); % Ox/Fuel ratio [-]
19 Pc(1) = nozzle_variables.nozzle_variables(4); % Initial CC pressure [Pa]
```

```

20 cF_tot = nozzle_variables.nozzle_variables(5); % Total Cf [-]
21 Lambda_RAO_2D = nozzle_variables.nozzle_variables(6); % 2D nozzle losses [-]
22
23 t_burn = 100; % Burn Time [s]
24
25 d1=3/16 * 25.4e-3; % Fuel feed line diameter [m]
26 d2=3/16 * 25.4e-3; % Ox feed line diameter [m]
27
28 dj1=0.372576e-3; % Fuel feed line diameter [m]
29 dj2=0.9026e-3; % Ox feed line diameter [m]
30
31 % Polytropic expansion of He in Ox-Fuel tanks choice:
32 % kHe = 1.66; % He Adiabatic Transformation
33 kHe = 1; % He Isothermal Transformation
34
35 RHe = 8.314/4; % He gas costant [J/kg*K]
36
37 mdot1(1) = Pc(1) * At / cstar*(1/(OFratio(1)+1)); % Initial Fuel Mass Flow ...
      Rate [kg/s]
38 mdot2(1) = Pc(1) * At / cstar*(OFratio(1)/(OFratio(1)+1)); % Initial Ox Mass Flow Rate ...
      [kg/s]
39
40 [K1,K2] = K_estim(mdot1(1)+mdot2(1), Pc(1), OFratio(1), d1, d2, dj1, dj2); % Fuel ...
      (K1), Ox(K2) Tubing losses
41
42 rho1 = 800.96; % Fuel Density [kg/m^3]
43 rho2 = 1308; % Ox Density [kg/m^3]
44
45 Tg1(1) = 298.15; % He initial fuel tank temperature [K]
46 Tg2(1) = 298.15; % He initial ox tank temperature [K]
47
48 Vp1(1) = (B^(1/kHe) - 1)*Vg1(1); % Fuel initial volume [m^3]
49 Vp2(1) = (B^(1/kHe) - 1)*Vg2(1); % Ox initial volume [m^3]
50 Mp1(1) = rho1 * Vp1(1); % Fuel initial mass [kg]
51 Mp2(1) = rho2 * Vp2(1); % Ox initial mass [kg]
52 P1(1) = K1*mdot1(1)^2+Pc(1); % Fuel tank initial pressure [Pa]
53 P2(1) = K2*mdot2(1)^2+Pc(1); % Ox tank initial pressure [Pa]
54
55 %% Time propagation
56
57 dt = 1e-1; % Time increment [s]
58 j = 1; % Index of increment
59 tb=0; % Initial time [s]
60
61 % Preallocation of variables for speed
62 mdot1 = [mdot1 zeros(size(dt:dt:t_burn))]; % Fuel Mass Flow Rate [kg/s]
63 mdot2 = [mdot2 zeros(size(dt:dt:t_burn))]; % Ox Mass Flow Rate [kg/s]
64 OFratio = [OFratio zeros(size(dt:dt:t_burn))]; % Ox/Fuel ratio [-]
65 Pc = [Pc zeros(size(dt:dt:t_burn))]; % CC Pressure [Pa]
66 Mp1 = [Mp1 zeros(size(dt:dt:t_burn))]; % Fuel mass (inside tank) [kg]
67 Mp2 = [Mp2 zeros(size(dt:dt:t_burn))]; % Ox mass (inside tank) [kg]
68 Vg1 = [Vg1 zeros(size(dt:dt:t_burn))]; % He volume in Fuel tank [m^3]
69 Vg2 = [Vg2 zeros(size(dt:dt:t_burn))]; % He volume in Ox tank [m^3]
70 Tg1 = [Tg1 zeros(size(dt:dt:t_burn))]; % He temperature in Fuel tank [K]
71 Tg2 = [Tg2 zeros(size(dt:dt:t_burn))]; % He temperature in Ox tank [K]
72 P1 = [P1 zeros(size(dt:dt:t_burn))]; % Pressure in Fuel tank [Pa]
73 P2 = [P2 zeros(size(dt:dt:t_burn))]; % Pressure in Ox tank [Pa]
74
75 while (Mp1(j)>0 && Mp2(j)>0 && tb<=t_burn)
76   % Integration in time until Burn time is reached or a propellant tank
    % is empty
77
78   Mp1(j+1) = Mp1(j) - dt * mdot1(j);
   Mp2(j+1) = Mp2(j) - dt * mdot2(j);
   Vg1(j+1) = Vg1(j) + dt * mdot1(j)/rho1;
   Vg2(j+1) = Vg2(j) + dt * mdot2(j)/rho2;
79
80   % polytropic transformation (adiabatic/isothermal)
81   Tg1(j+1) = Tg1(j) * (Vg1(j)/Vg1(j+1))^(kHe-1);
82   Tg2(j+1) = Tg2(j) * (Vg2(j)/Vg2(j+1))^(kHe-1);
83   P1(j+1) = P1(j)*(Vg1(j)/Vg1(j+1))^kHe;
84   P2(j+1) = P2(j)*(Vg2(j)/Vg2(j+1))^kHe;
85
86
87
88
89
```

```

90      % Computation of mass flow rates and CC pressure
91      F=@(x) root3d(x,P1(j+1),P2(j+1),K1,K2,At,cstar);
92      x0=[mdot1(j) mdot2(j) Pc(j)]';
93      options = optimset('Display','off');
94      X = fsolve (F,x0,options);
95      mdot1(j+1)=X(1);
96      mdot2(j+1)=X(2);
97      Pc(j+1)=X(3);
98
99      % Check of O/F ratio
100     OFratio(j+1) = mdot2(j)/mdot1(j);
101
102    j = j + 1;
103    tb = dt * j;
104 end
105
106 T = Pc.*cF_tot.*At.*Lambda_RAO_2D;           % Thrust [N]
107
108 MHe1= P1(1)*Vg1(1)/RHe/Tg1(1);             % He mass in Fuel tank [kg]
109 MHe2= P2(1)*Vg2(1)/RHe/Tg2(1);             % He mass in Ox tank [kg]
110
111 % Fuel tank - spherical shape - material AISI 316
112 V1          = Vp1(1) + Vg1(1);                 % Total Fuel tank volume [m^3]
113 sigma_acc  = 200e6;                          % AISI 316 Yield strength [Pa]
114 safety_f   = 1.15;                           % Safety factor
115 r1          = (3*V1/4/pi)^(1/3);            % Internal tank radius [m]
116 th1         = r1*P1(1)/2/sigma_acc*safety_f; % Wall thickness of tank [m]
117
118 % Oxidant tank - Cylindrical shape - material AISI 316
119 V2          = Vp2(1) + Vg2(1);                 % Total Ox tank volume [m^3]
120 r2          = r1;                            % Internal tank radius [m]
121 A_cyl       = r2^2*pi;                      % Cylinder cross section [m^2]
122 l_cyl       = (V2-4/3*pi*r2^3)/A_cyl;        % Length of cylindrical section [m]
123 th2         = r2*P2(1)/sigma_acc*safety_f; % Wall thickness of cyl tank [m]
124
125 %% Postprocess
126
127 fprintf("Burn time: %d s\n", tb)
128 fprintf("Fuel mass: %d kg \nExtra Fuel: %d kg \n", Mp1(1),Mp1(end))
129 fprintf("Ox mass: %d kg \nExtra Ox: %d kg \n", Mp2(1),Mp2(end))
130 fprintf("V Fuel Tank: %d m^3 \nV Oxidant Tank: %d m^3\n",V1,V2)
131
132 tt = (0:dt:t_burn);
133
134 figure
135 title("Performance parameters over time")
136
137 subplot(2,2,1)
138 plot(tt,T,LineWidth=2)
139 grid on
140 ylabel("Vacuum thrust [N]")
141 xlabel("Time [s]")
142
143 subplot(2,2,2)
144 plot(tt,OFratio-7.5,LineWidth=2)
145 grid on
146 ylabel("O/F ratio error")
147 xlabel("Time [s]")
148
149 subplot(2,2,3)
150 plot(tt,mdot1+mdot2,LineWidth=2)
151 grid on
152 ylabel("Prop flow rate [kg/s]")
153 xlabel("Time [s]")
154
155 subplot(2,2,4)
156 plot(tt,Pc*1e-5,tt,P1*1e-5,tt,P2*1e-5,LineWidth=2)
157 grid on
158 ylabel("Pressure [bar]")
159 xlabel("Time [s]")
160 legend('P_C_C','P_f_u_e_l','P_o_x')

```

### E.2.3 Tanks sizing

The last part of the blowdown script makes also the mechanical sizing of the propellant tanks. Due to the big O/F ratio the oxidizer tank was bigger than the fuel one, so has been chosen to design a spherical tank for the fuel and to use instead a cylindrical type tank for the oxidizer, keeping the same radius for both tanks to reduce the cross section area of the propulsion system.

Once the internal dimensions have been defined the thickness of the walls have been sized using the Mariotte Formula, since the ratio between thickness and tank radius was really below 1 and the thin wall approximation was valid.

A yield strength of AISI 316 of 200 MPa has been selected and a safety factor of 1.15 has been applied to obtain the maximum admissible strength of tanks' material.

-	Tank radius	Tank length	Thickness <sub>fuel</sub>	Thickness <sub>ox</sub>
[mm]	58.6	279.3	0.4	0.8

Table E.1: Tanks sizing results

## E.3 Optimization of initial variables

### E.3.1 Variables

```

1 B      = x(1);      % Blowdown ratio
2 Vg1    = x(2);      % Initial GHe volume in fuel tank
3 Vg2    = x(3);      % Initial GHe volume in oxidizer tank
4
5 %% Data
6
7 nozzle_variables = load('nozzle_variables.mat','nozzle_variables');
8 At      = nozzle_variables.nozzle_variables(1);
9 cstar   = nozzle_variables.nozzle_variables(2);
10 OFratio(1) = nozzle_variables.nozzle_variables(3);
11 Pc(1)   = nozzle_variables.nozzle_variables(4);
12 cF_tot = nozzle_variables.nozzle_variables(5);
13 Lambda_RAO_2D = nozzle_variables.nozzle_variables(6);
14
15 d1=3/16 * 25.4e-3;
16 d2=3/16 * 25.4e-3;
17
18 dj1=0.372576e-3;          % Fuel feed line diameter [m]
19 dj2=0.9026e-3;           % Ox feed line diameter [m]
20
21 % Target
22
23 Tg2end_target = 273.15-10; % Final He temperature in the Ox tank [K]
24 M_margin=0.10;             % % of propellant to mantain until mission ending
25 M_tol=0.01;                % % of tolerance on masses
26 Tend = 60;                 % Final thrust [N]
27 T_tol=0.01;                % % of tolerance on thrust

```

### E.3.2 Variables' ranges

```

1 range(:, idx.B)      = [1      1.4105      4];
2 range(:, idx.Vg1)    = [1e-4   0.0020224 1e-1];
3 range(:, idx.Vg2)    = [1e-4   0.0092777 1e-1];

```

### E.3.3 Constraints

```
1 c = [abs(Mp1(end)-M_margin*Mp1(1))-M_tol*Mp1(1); ...
2      abs(Mp2(end)-M_margin*Mp2(1))-M_tol*Mp2(1); ...
3      abs(Tend-T(end))-T_tol*T(1)]; ...
4 ceq = [];
```

### E.3.4 Objective function

```
1 f = norm(abs(OFratio-7.5))+Vg1(1)+Vg2(1);
```

### E.3.5 Optimizer

```
1 %% Boundaries
2
3 % Allocate values of lb and ub on range matrix
4 lb = range(1, :);
5 ub = range(3, :);
6
7 %% Choosing of x0
8 % 1. Allocate values of x0 from range matrix
9 % x0 = range(2, :);
10
11 % 2. Allocate values of x0 from random values inside the boundaries of the range matrix
12 % x0 = range(1, :) + (range(3, :)-range(1, :)).*rand(size(lb));
13
14 % 3. Choose x0 as solution of a previously optimization
15 load('Results\Prova3_AAR\Prova3_AAR.mat');
16 x0 = x;
17
18 %% Optimization
19
20 %rng default % Permits the repeatability of the optimization
21 % (deactivate to see other solutions)
22
23 % Genetic algorithm
24 %[x,fval,exitflag,output] = ga(@fitness, nvar, lin_coeff, t_noti, lin_coeff_eq, ...
25 % t_noti_eq, lb, ub, @constr, IntVar, options_ga)
26
27 % Surrogate algorithm
28 %[x,fval,exitflag,output] = surrogateopt(@objective, lb, ub, IntVar, options_sur)
29
30 % Gradient algorithm
31 [x,fval,exitflag,output] = fmincon(@fitness, x0, lin_coeff, t_noti, lin_coeff_eq ...
, t_noti_eq, lb, ub, @constr, options_f)
32 save('x.mat','x');
```

# Appendix F

## Statistical analysis

### F.1 Montecarlo initialization and post-processing

```
1 clear
2 clc
3 close all
4
5 tic
6
7 rng('shuffle')
8
9 it = 1e3;
10
11 figure
12 subplot(2,3,[1 4])
13 grid on
14 hold on
15 ylabel("Tvac [N]")
16 xlabel("Time [s]")
17
18 xlim([0 100])
19
20 Tmean = zeros(1,it);
21 Tesigma = zeros(1,it-1);
22
23 for i = 1:it
24     [T,tt] = blowdown_sim;
25     perc_old = floor((i-1)/it*100);
26     perc_new = floor(i/it*100);
27     plot(tt,T,LineWidth=2,Color=[0.4940 0.1840 0.5560])
28     if perc_new > perc_old
29         fprintf("SIMULATION PROGRESS: %d percent\n", perc_new)
30     end
31     Tstart(i) = T(1);
32     Tend(i) = T(end);
33     Tsmean(i) = sum(Tstart)/i;
34     Tmean(i) = sum(Tend)/i;
35     if i≥2
36         Tssigma(i-1) = std(Tstart);
37         Tesigma(i-1) = std(Tend);
38     end
39 end
40
41 subplot(2,3,2)
42 plot(Tsmean,LineWidth=2)
43 grid on
44 hold on
45 Tsmax = max(Tstart);
46 Tsmin = min(Tstart);
47 plot([0 it],[Tsmax Tsmax],LineWidth=2,Color='k')
48 plot([0 it],[Tsmin Tsmin],LineWidth=2,Color='k')
49 xlabel("Iterations")
50 ylabel("Mean of starting Tvac [N]")
51 subplot(2,3,5)
52 plot(Tmean,LineWidth=2,Color=[0.8500 0.3250 0.0980])
53 grid on
54 hold on
55 Temax = max(Tend);
```

```

56 Temin = min(Tend);
57 plot([0 it],[Temax Temax],LineWidth=2,Color='k')
58 plot([0 it],[Temin Temin],LineWidth=2,Color='k')
59 xlabel("Iterations")
60 ylabel("Mean of final Tvac [N]")
61 subplot(2,3,[3 6])
62 % plot(Tssigma/Tsmean(end),LineWidth=2)
63 plot(Tssigma,LineWidth=2)
64 grid on
65 hold on
66 % plot(Tesigma/Temean(end),LineWidth=2,Color=[0.8500 0.3250 0.0980])
67 plot(Tesigma,LineWidth=2,Color=[0.8500 0.3250 0.0980])
68 % plot({})
69 xlabel("Iterations")
70 ylabel("Std of Tvac[N]")
71 legend("Tstart","Tend")
72
73 toc

```

## F.2 Simulation with uncertainties

```

1 function [T,tt] = blowdown_sim
2
3 %% UNCOMMENT OR COMMENT THE RANDN FUNCTIONS TO ADD/REMOVE DEVIATIONS
4
5 %% Variables
6
7 %----- Variables from Optimization -----
8 B=1.9048; % Blowdown ratio [-]
9 Vg1(1) = 0.00044221; % He Fuel tank initial volume [m^3]
10 Vg2(1) = 0.0020233; % He Ox tank initial volume [m^3]
11 %
12
13 nozzle_variables = load('nozzle_variables.mat','nozzle_variables');
14 At = nozzle_variables.nozzle_variables(1); % Throat area [m^2]
15 cstar = nozzle_variables.nozzle_variables(2); % C* [m/s]
16 OFratio(1) = nozzle_variables.nozzle_variables(3); % Ox/Fuel ratio [-]
17 Pc(1) = nozzle_variables.nozzle_variables(4); % Initial CC pressure [Pa]
18 cF_tot = nozzle_variables.nozzle_variables(5); % Total Cf [-]
19 Lambda_RAO_2D = nozzle_variables.nozzle_variables(6); % 2D nozzle losses [-]
20
21 t_burn = 100; % Burn Time [s]
22
23 d_tinc = 2e-6;
24 d_t = (At*4/pi)^0.5+randn(1)*d_tinc;
25
26 At = d_t^2 * pi/4;
27
28 Pc(1) = Pc(1);%*(1 + randn(1)*0.1/Pc(1));
29
30 d_12inc = 1e-4;
31 d1=3/16 * 25.4e-3+randn(1)*d_12inc; % Fuel feed line diameter [m]
32 d2=3/16 * 25.4e-3+randn(1)*d_12inc; % Ox feed line diameter [m]
33
34 dj_inc = 1e-6;
35 dj1 = 0.372576e-3 +randn(1)*dj_inc;
36 dj2 = 0.9026e-3 +randn(1)*dj_inc;
37
38 % Polytropic expansion of He in Ox-Fuel tanks choice:
39 % kHe = 1.66; % He Adiabatic Transformation
40 kHe = 1;%*(1+abs(randn(1)*0.03)); % He Isothermal Transformation
41
42 % RHe = 8.314/4; % He gas costant [J/kg*K]
43
44 mdot1(1) = Pc(1) * At / cstar*(1/(OFratio(1)+1)); % Initial Fuel Mass Flow ...
        Rate [kg/s]
45 mdot2(1) = Pc(1) * At / cstar*(OFratio(1)/(OFratio(1)+1)); % Initial Ox Mass Flow Rate ...
        [kg/s]
46

```

```

47 [K1,K2] = K.estim(mdot1(1)+mdot2(1), Pc(1), OFratio(1), d1, d2, dj1, dj2); % Fuel ...
    (K1), Ox(K2) Tubing losses
48
49 rho1 = 800.96; % Fuel Density [kg/m^3]
50 rho2 = 1308; % Ox Density [kg/m^3]
51
52 %T_dev = randn(1)*5;
53 Tg1(1) = 298.15;% + T_dev; % He initial fuel tank temperature [K]
54 Tg2(1) = 298.15;% + T_dev; % He initial ox tank temperature [K]
55
56 Vp1(1) = (B^(1/kHe) - 1)*Vg1(1); % Fuel initial volume [m^3]
57 Vp2(1) = (B^(1/kHe) - 1)*Vg2(1); % Ox initial volume [m^3]
58 Mp1(1) = rho1 * Vp1(1); % Fuel initial mass [kg]
59 Mp2(1) = rho2 * Vp2(1); % Ox initial mass [kg]
60 P1(1) = K1*mdot1(1)^2+Pc(1); % Fuel tank initial pressure [Pa]
61 P2(1) = K2*mdot2(1)^2+Pc(1); % Ox tank initial pressure [Pa]
62
63 %% Time propagation
64
65 dt = 1e-1; % Time increment [s]
66 j = 1; % Index of increment
67 tb=0; % Initial time [s]
68
69 % Preallocation of variables for speed
70 mdot1 = [mdot1 zeros(size(dt:dt:t_burn))]; % Fuel Mass Flow Rate [kg/s]
71 mdot2 = [mdot2 zeros(size(dt:dt:t_burn))]; % Ox Mass Flow Rate [kg/s]
72 OFratio = [OFratio zeros(size(dt:dt:t_burn))]; % Ox/Fuel ratio [-]
73 Pc = [Pc zeros(size(dt:dt:t_burn))]; % CC Pressure [Pa]
74 Mp1 = [Mp1 zeros(size(dt:dt:t_burn))]; % Fuel mass (inside tank) [kg]
75 Mp2 = [Mp2 zeros(size(dt:dt:t_burn))]; % Ox mass (inside tank) [kg]
76 Vg1 = [Vg1 zeros(size(dt:dt:t_burn))]; % He volume in Fuel tank [m^3]
77 Vg2 = [Vg2 zeros(size(dt:dt:t_burn))]; % He volume in Ox tank [m^3]
78 Tg1 = [Tg1 zeros(size(dt:dt:t_burn))]; % He temperature in Fuel tank [K]
79 Tg2 = [Tg2 zeros(size(dt:dt:t_burn))]; % He temperature in Ox tank [K]
80 P1 = [P1 zeros(size(dt:dt:t_burn))]; % Pressure in Fuel tank [Pa]
81 P2 = [P2 zeros(size(dt:dt:t_burn))]; % Pressure in Ox tank [Pa]
82
83 while (Mp1(j)>0 && Mp2(j)>0 && tb<t_burn)
    % Integration in time until Burn time is reached or a propellant tank
    % is empty
84
85
86
87 Mp1(j+1) = Mp1(j) - dt * mdot1(j);
88 Mp2(j+1) = Mp2(j) - dt * mdot2(j);
89 Vg1(j+1) = Vg1(j) + dt * mdot1(j)/rho1;
90 Vg2(j+1) = Vg2(j) + dt * mdot2(j)/rho2;
91
92 % polytropic transformation (adiabatic/isothermal)
93 Tg1(j+1) = Tg1(j) * (Vg1(j)/Vg1(j+1))^(kHe-1);
94 Tg2(j+1) = Tg2(j) * (Vg2(j)/Vg2(j+1))^(kHe-1);
95 P1(j+1) = P1(j)*(Vg1(j)/Vg1(j+1))^kHe;
96 P2(j+1) = P2(j)*(Vg2(j)/Vg2(j+1))^kHe;
97
98 % Computation of mass flow rates and CC pressure
99 F=@(x) root3d(x,P1(j+1),P2(j+1),K1,K2,At,cstar);
100 x0=[mdot1(j) mdot2(j) Pc(j)'];
101 options = optimset('Display','off');
102 X = fsolve(F,x0,options);
103 mdot1(j+1)=X(1);
104 mdot2(j+1)=X(2);
105 Pc(j+1)=X(3);
106
107 % Check of O/F ratio
108 OFratio(j+1) = mdot2(j)/mdot1(j);
109
110 j = j + 1;
111 tb = dt * j;
112 end
113
114 T = Pc.*cF_tot.*At.*Lambda_RAO_2D; % Thrust [N]
115 tt = (0:dt:t_burn);

```

### F.3 Results of the sensitivity analysis

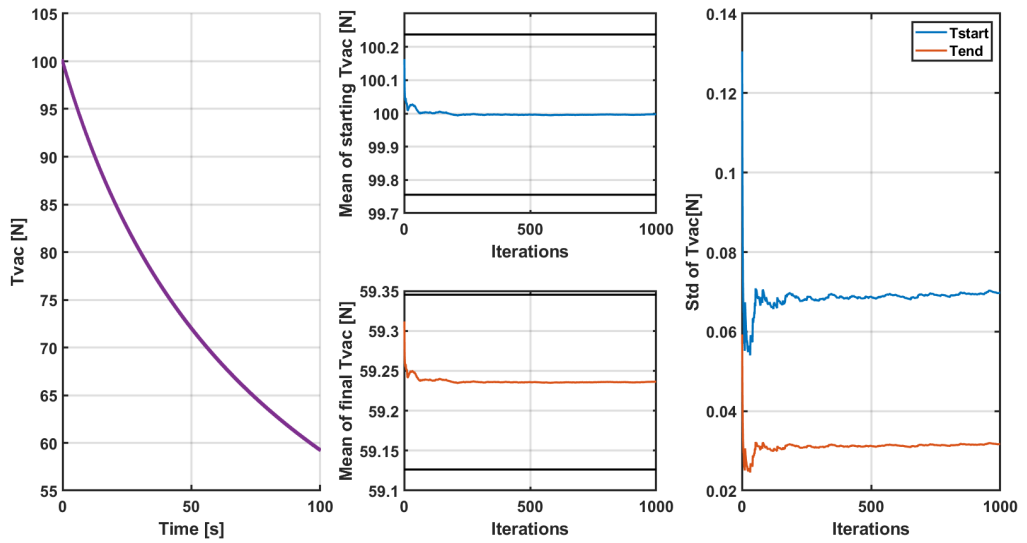


Figure F.1: Throat diameter as variable parameter REFINED

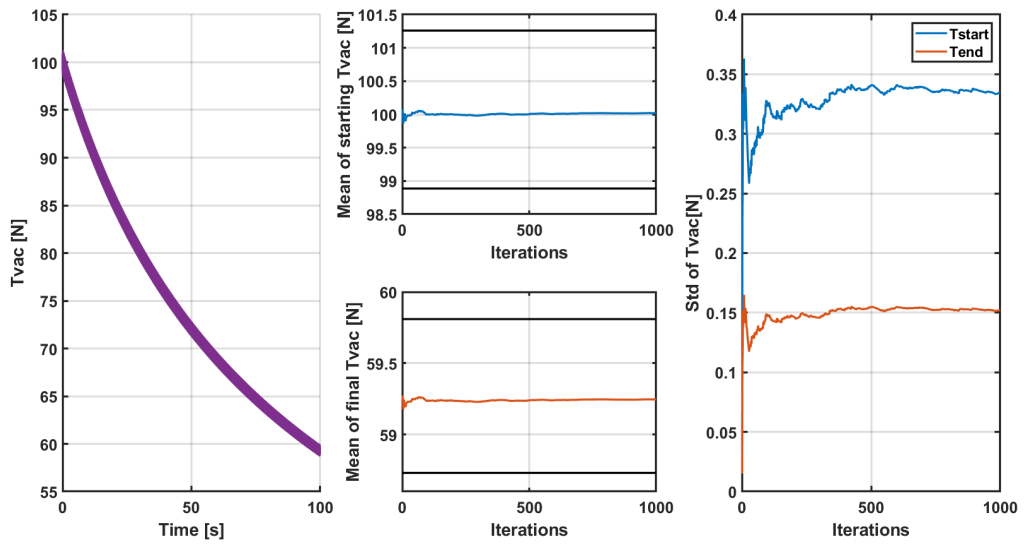


Figure F.2: Throat diameter as variable parameter NOT REFINED

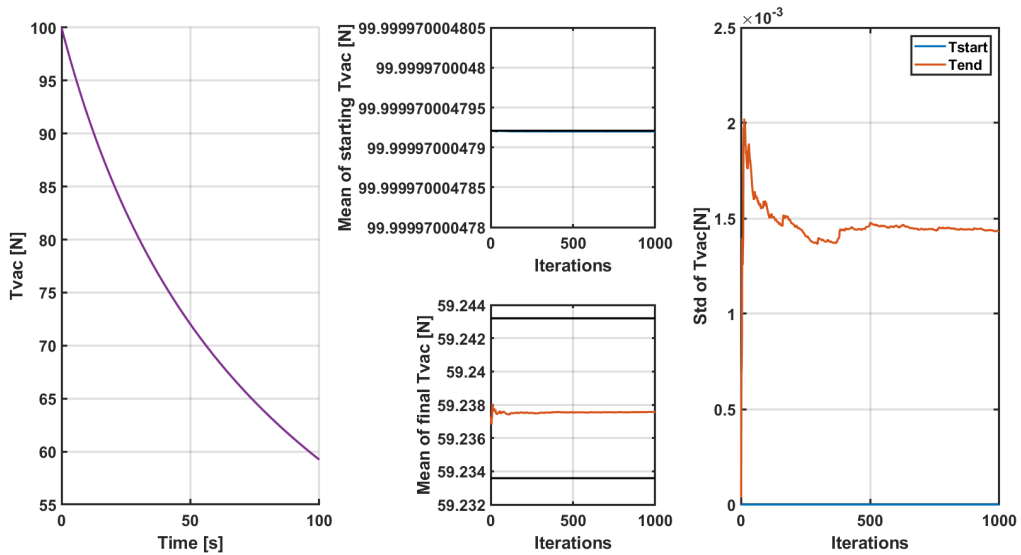


Figure F.3: Feeding lines diameter as variable parameter

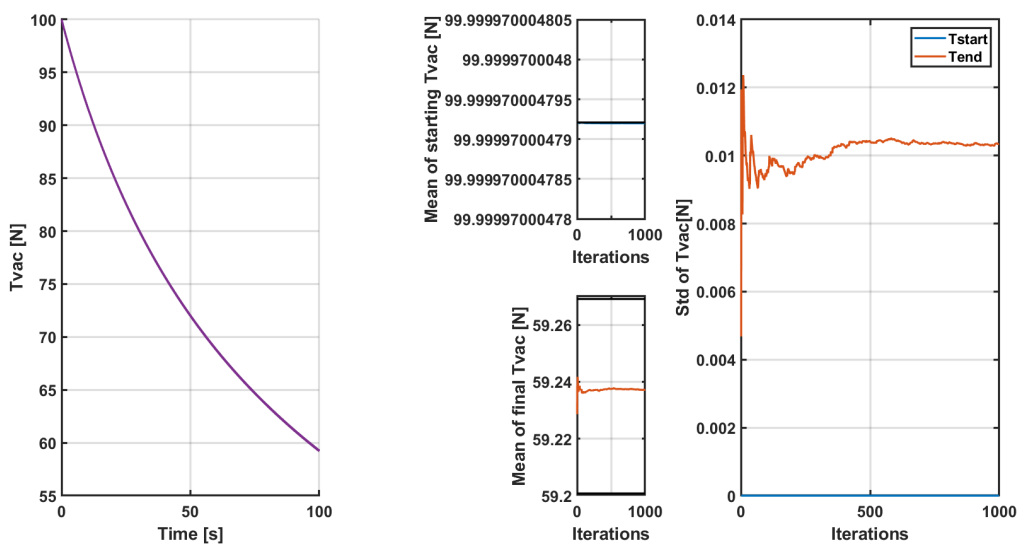


Figure F.4: Injectors diameters as variable parameter